LOCAL DISCRETE VELOCITY GRIDS FOR MULTI-SPECIES RAREFIED FLOW SIMULATIONS

STÉPHANE BRULL AND CORENTIN PRIGENT

Abstract. This article deals with the derivation of an adaptive numerical method for mono-dimensional kinetic equations for gas mixtures. For classical deterministic kinetic methods, the velocity domain is chosen accordingly to the initial condition. In such methods, this velocity domain is the same for all time, all space points and all species. The idea developed in this article relies on defining velocity domains that depend on space, time and species. This allows the method to locally adapt to the support of the distribution functions. The method consists in computing macroscopic quantities by the use of conservation laws, which enables the definition of such local grids. Then, an interpolation procedure along with a upwind scheme is performed in order to treat the advection term, and an implicit treatment of the BGK operator allows for the derivation of an AP scheme, where the stability condition is independant of the relaxation rate. The method is then applied to a series of test case and compared to the classical DVM method.

1. Introduction

In the process of designing vehicules such as aircrafts, it is necessary to study gas mixture dynamics in rarefied configurations. In such cases, systems of PDEs such as Euler or Navier-Stokes equations may not be suitable when the Knudsen number, describing the level of rarefaction of a gas, becomes important. To this end, kinetic models, involving distribution functions defined over the phase space - a space with a larger dimension than the physical one -, need to be used. These equations, much more general and more accurate than the so-called fluid models, allow for the modelling of any level of rarefied gas.

However, in the context of numerical simulations, accuracy is obtained in exchange for computational cost. More specifically, in a general d-dimensional configuration, the kinetic variable, denoted v, ranges over all $\mathbb{R}^d$. Hence, in order to perform numerical approximations, the definition domain of v needs to be replaced by a bounded subset of $\mathbb{R}^d$ which contains most of the information. Close to thermodynamical equilibrium, macroscopic quantitites (velocities and temperatures) can be used to determine the bounds of such a subset. However, since the bounds depend on the macroscopic quantities, that themselves depend on the physical point $x \in \mathbb{R}^d$ considered, the suitable subset can vary greatly from one physical point to the other, especially through shock waves. Besides, from one species to the other, the disparities of particle masses lead to different bounds, even in the case of equivalent velocities and temperatures. Finally, quantities at a point can also vary importantly over time.

In classical numerical methods, one grid is usually taken for all physical points and all species, for all time, based on the initial data. This implies that this grid has large enough bounds to encompass the broadest distribution, and that it is precise enough in order to "see" the narrowest one.

In this article, an adaptive numerical method is proposed for multi-species kinetic equations. Such a method is able to use a different velocity grid for each physical point and each gas species, and is also adaptive in time. The idea is to use conservation laws, at each time step, in order to compute macroscopic quantites beforehand. These quantities, depending on space, time and species, are then used to define a velocity grid suitable at the subsequent discrete time. Moreover, the computation of these macroscopic quantities allows for the implicit treatment of the relaxation operator modelling collisions, which gives an asymptotic-preserving scheme for Euler in the case

of a Knudsen number tending to zero. Once local velocity grids are computed, in order to apply a upwind scheme to the distribution functions, since every quantity is defined on its own grid, it is necessary to perform an interpolation procedure. This is done by using a ENO4 interpolation method, which consists in choosing an interpolation stencil with the smallest variation rate of the solution. This method prevents the interpolation through discontinuities, which can degrade the quality of the method. A second version of the method is proposed, where velocity grids are chosen in order to avoid interpolations. This is done by choosing grids with steps that are all multiple of the same quantity, so that they possess an important amount of common velocities, where interpolating is then not required. This allows for a decrease of computational cost when the number of prevented interpolations is great.

Collisions in a multi-species gas are modeled by the multi-species Boltzmann operator, presented for example in [13], [2] or [27]. However, for numerical purposes, it is more interesting to replace the Boltzmann operator by a simpler relaxation term. In the case of mono-species gas, the well-known Bhatnagar-Gross-Krook model [5] ensures all the fundamental properties of the mono-species Boltzmann operator (positivity of the solution, conservation of moments, dissipation of entropy). However, in the multi-species case, modelling is a more complicated problem. More precisely, in the multi-species case, more properties may be needed in order to model collisions correctly. For example, models can be required to fit the correct macroscopic coefficients in the hydrodynamic limit of the kinetic equations, that are more numerous than for the mono-species case. The Fick coefficients, or the Soret and Dufour effects, which describe different types of diffusion between components of the gas, are examples of these coefficients that do not exist in the mono-species case. Other parameters such as the cross-section of collisions, or the correctness of the momentum and energy exchange terms between species, or the indifferentiability principle (which ensures that, when particle masses and cross-sections are all equal, the model is reduced to the classical mono-species model), can be the basis for the derivation of a model. Different classes of models exist in order to approximate these terms. The first attempts trace back to the decades 1960-70, with the models of Gross-Krook, Hamel, Sirovich, Morse and McCormack ([17],[19],[32],[30], [29]). Then, several other models have been developped such as the Andries-Aoki-Perthame model [1], the Kosuge model [26], the Brull-Pavan-Schneider model [11], the Brull ellipsoidal model [8], the model by Haack-Hauck-Murillo [18]. One can also refer to the recent works by Bobylev et al. [7] and Klingenberg et al. [24]. In this article, the model considered is the Andries-Aoki-Perthame model [1], its main property being that it models the correct momentum and energy exchange terms between species. An advantage of this model is its simplicity, since it consists in a relaxation operator towards only one equilibrium distribution similar to the classical BGK operator. This means that, as is developped in this article, the implicit treatment of this term is easily performed, as a consequence of the adaptive method.

Numerical resolution of mixture kinetic equations has been investigated in several recent works. In [21], a Fast Fourier spectral method is applied to compare the results of Boltzmann model and the McCormack model. In [37], [36], [33], [34], [28], the Discrete Unified Gas Kinetic Scheme (DUGKS) is extended to multi-species flows described by several multi-species models. Then, a Discontinuous Galerkin (DG) approach has been applied to the Boltzmann equations in [23] and [22].

Concerning adaptive methods for kinetic flows, several authors have studied the problems for a range of different types of applications. In [14], the DUGKS method is extended to an adaptive velocity method. Filbet and Rey proposed in [16] a method based on the rescaling of velocity domains. Procedures involving the use of quad-trees and octrees have been widely investigated by Arslanbekov and Kolobov in [3], [25] and [35]. Finally, Bernard et al. developed an approach to obtain adaptive velocity meshes with constant spacings [4].

The article is organized as follows. In section 2, the Boltzmann model is presented, along with the Andries-Aoki-Perthame model used in the numerical method. Then, in section 3, a first version of the numerical method, based on the work done in [10], is presented in detail. In section 4, the second version of the method, an adaptive method where the local velocity grids are chosen

in order to diminish the number of interpolations, is presented. Finally, numerical experiments are conducted in section 5, in order to validate the method and compare its efficiency to the classical DVM method.

2. Multi-species kinetic model for rarefied flows

2.1. **Multi-species Boltzmann equation.** A gas mixture composed of N species can be modeled by the following three-dimensional multi-species Boltzmann equations, for $\alpha \in \{1, ..., N\}$:

$$\partial_t f^\alpha + \nabla.(v f^\alpha) = \mathcal{Q}^\alpha(f), \qquad t \in \mathbb{R}_+, \qquad x \in \Omega \subset \mathbb{R}^3, \qquad v \in \mathbb{R}^3,$$

where $f^\alpha(t, x, v) : \mathbb{R}_+ \times \Omega \times \mathbb{R} \mapsto \mathbb{R}_+$ is the distribution function of species α, which represents the number of particles of species α.

On the r.h.s of the equation, $\mathcal{Q}^\alpha$ is the source term modelling collisions between particles, defined by

$$\mathcal{Q}^\alpha(f) = \sum_{\beta=1}^{N} \mathcal{Q}^{\alpha\beta}(f^\alpha, f^\beta) = \sum_{\beta=1}^{N} \int_{\mathbb{R}^3} \int_{S_2} ((f^\alpha)'(f_*^\beta)' - f^\alpha f_*^\beta) B^{\alpha\beta}(n.V, |V|) \mathrm{d}n \mathrm{d}v^*, \tag{1}$$

with $f_*^\beta = f^\beta(t, x, v_*), (f^\alpha)' = f^\alpha(t, x, v'), (f_*^\beta)' = f^\beta(t, x, v'_*)$, where v and v_* are the precollisional velocities of a given binary encounter, and v' and v'_* are the corresponding postcollisional velocities, given by

$$v' = v - 2\frac{\mu^{\alpha\beta}}{m^\alpha}(V.n)n,$$
$$v'_* = v_* + 2\frac{\mu^{\alpha\beta}}{m^\beta}(V.n)n,$$

where $\mu^{\alpha\beta} = \frac{m^\alpha m^\beta}{m^\alpha + m^\beta}$ is the reduced mass, n is the unit vector joining the centers of the two colliding spheres and $V = v - v_*$ is the relative velocity. The domain of integration w.r.t n is S_2, the 2-dimensional sphere defined by $n.V = 0$, and $B^{\alpha\beta}(n.V, |V|)$ is the collision kernel of $\alpha - \beta$ collisions. Hereafter, only Maxwellian molecules will be considered. This means that the collision kernel is independant of the amplitude of the relative velocity $|V|$, which can then be written as follows

$$B^{\alpha\beta}(n.V, |V|) = \bar{B}^{\alpha\beta}(\omega), \qquad \omega = \frac{n.V}{|V|}.$$

Define the following quantities relative to the collision kernel, which will be useful later:

$$\chi^{\alpha\beta} = \int_{S_2} \cos(\omega)^2 \bar{B}^{\alpha\beta}(\omega) \mathrm{d}\omega, \tag{2a}$$

$$\nu^{\alpha\beta} = \int_{S_2} \bar{B}^{\alpha\beta}(\omega) \mathrm{d}\omega. \tag{2b}$$

In this article, we are interested in the numerical resolution of the mono-dimensional equations for multi-species rarefied flows. The physical domain is denoted $\Omega = [L_{\min}, L_{\max}]$, with $L_{\min}, L_{\max} \in \mathbb{R}$. The equation reads, for $\alpha \in \{1, ..., N\}$:

$$\partial_t f^\alpha + \partial_x (v f^\alpha) = \tilde{\mathcal{Q}}^\alpha, \qquad t \in \mathbb{R}_+, \qquad x \in [L_{\min}, L_{\max}], \qquad v \in \mathbb{R}, \tag{3}$$

where $\tilde{\mathcal{Q}}^\alpha$ is an operator modelling collisions in one dimension. Even though the Boltzmann operator is not defined in 1D, simplified operators such as the ones discussed in the following section can still be defined.

2.2. **Macroscopic quantities.** Macroscopic quantities, that are unknowns of fluid equations such as Euler or Navier-Stokes, are defined as moments of the distribution functions. For any function g that depends on v such that $(1+v^2)g \in L^1(\mathbb{R})$, denote

$$\langle g \rangle = \int_{\mathbb{R}} g \mathrm{d}v.$$

The concentration, velocity and temperature of species α, denoted respectively n^α, u^α and T^α, are defined through the first three moments of f^α:

$$\begin{aligned}
&\langle f^\alpha \rangle = n^\alpha, \\
&\langle m^\alpha v f^\alpha \rangle = m^\alpha n^\alpha u^\alpha = \rho^\alpha u^\alpha, \\
&\langle m^\alpha \frac{v^2}{2} f^\alpha \rangle = E^\alpha = \frac{1}{2} m^\alpha n^\alpha (u^\alpha)^2 + n^\alpha \varepsilon^\alpha = \frac{1}{2} m^\alpha n^\alpha (u^\alpha)^2 + \frac{1}{2} n^\alpha k_B T^\alpha,
\end{aligned}$$

where E^α and ε^α denote respectively the total energy and the internal energy of species α.

2.3. **Multi-species BGK model.** For numerical purposes, it is convenient to replace the Boltzmann collision operator by another operator, which is easier to treat numerically. For multi-species flows, several models exist, each with different modelling properties. In this article, the choice is made to use the BGK-type operator derived in [1] by Andries, Aoki and Perthame. Hence, using these notations from the previous section, define the following relaxation operator as an approximation of $\tilde{\mathcal{Q}}^\alpha$

$$\tilde{\mathcal{Q}}^\alpha := \nu^\alpha (\overline{M}^\alpha(f) - f^\alpha), \tag{4}$$

where the relaxation frequency is defined as $\nu^\alpha = \sum_{\beta=1}^{N} \nu^{\alpha\beta} n^\beta$.

This operator models multi-species collisions with only one BGK-type relaxation towards a Maxwellian $\overline{M}^\alpha$, which is defined as

$$\overline{M}^\alpha(f) = \frac{n^\alpha}{\sqrt{2\pi k_B \frac{\overline{T}^\alpha}{m^\alpha}}} \exp\left(-\frac{(v-\overline{u}^\alpha)^2}{2k_B \frac{\overline{T}^\alpha}{m^\alpha}}\right), \tag{5}$$

where k_B denotes the Boltzmann constant. Mixture (or fictitious) moments, denoted $\overline{u}^\alpha$ and $\overline{T}^\alpha$, defined in equations (6) and (7), are quantities chosen so that the momentum and energy of the BGK operator (4) are equal to those of the actual Boltzmann operator for Maxwellian molecules (1), defined in the previous section (see [1] for more details). Their expression is the following:

$$\nu^\alpha m^\alpha \overline{u}^\alpha = \nu^\alpha m^\alpha u^\alpha + 2 \sum_{\beta=1}^{N} \mu^{\alpha\beta} \chi^{\alpha\beta} n^\beta \left(u^\beta - u^\alpha\right), \tag{6}$$

$$\overline{\varepsilon}^\alpha = \varepsilon^\alpha - \frac{m^\alpha}{2}(\overline{u}^\alpha - u^\alpha)^2 + \frac{2}{\nu^\alpha} \sum_{\beta=1}^{N} \mu^{\alpha\beta} \chi^{\alpha\beta} n^\beta \frac{2}{m^\alpha + m^\beta} \left(\varepsilon^\beta - \varepsilon^\alpha + m^\beta \frac{(u^\beta - u^\alpha)^2}{2}\right), \tag{7}$$

where $\overline{\varepsilon}^\alpha$ is the mixture internal energy, defined by $\overline{\varepsilon}^\alpha = \frac{1}{2} k_B \overline{T}^\alpha$ and $\chi^{\alpha\beta}$ is the interaction coefficient between species α and β defined in (2a).

These expressions of $\overline{u}^\alpha$ and $\overline{T}^\alpha$ are shown to ensure positivity of the internal energy (and hence, positivity of temperature) under the following condition on ν^α:

$$\nu^\alpha \geq \sum_{\beta=1}^{N} \chi^{\alpha\beta} n^\beta.$$

Hence, according to their definitions, $\chi^{\alpha\beta} \leq \nu^{\alpha\beta}$, which ensure the well-posedness of the model with the total frequency $\nu^\alpha = \sum_{\beta=1}^{N} \nu^{\alpha\beta} n^\beta$.

2.4. **Computation of the relaxation rates and interaction coefficients.** For numerical simulations, in order to select the regime of the flow under consideration, it is convenient to directly choose the value of the Knudsen number, defined as $K_n = \frac{\delta}{L}$, where δ is the mean free path of the molecules constituting the gas, and L is a typical length of the physical domain. Hence, as $K_n \to 0$, the kinetic equations tends to Euler equations. According to each definition, the value of the mean free path is directly related to the amount of collisions between particles in the gas. Then, it should depend on the value of the interaction parameters $\chi^{\alpha\beta}$ and $\nu^{\alpha\beta}$. However, as stated by Bird in [6], defining the Knudsen number of a gas mixture is not an easy matter. Hence, in this article, similarly to [26], the choice is made to define the Knudsen number of the mixture as the Knudsen number of a pure gas of a reference component (chosen as species 1 here). This allows for the definition of quantity ν^{11}, and the remaining quantities are then defined via dimensionless expressions. More precisely, the mean free path is defined as

$$\delta = \frac{1}{\nu^{11} n_0^1} \sqrt{\frac{8 k_B T_0^1}{\pi m^1}},$$

where T_0^1 and n_0^1 are respectively reference temperature and reference concentration of species 1. The length L will be chosen as the length of the physical domain, which will be equal to 1 in the cases shown below. Then, one obtains the following expression for ν^{11}:

$$\nu^{11} = \frac{1}{K_n n_0^1} \sqrt{\frac{8 k_B T_0^1}{\pi m^1}}.$$

According to [26] and [12], the collision kernel for Maxwellian molecules can be written under the following form:

$$B^{\alpha\beta}(\theta) = (\frac{a^{\alpha\beta}}{\mu^{\alpha\beta}})^{\frac{1}{2}} \frac{g(\theta)}{\sin(\theta)} \frac{\mathrm{d}g}{\mathrm{d}\theta}, \qquad \theta = \arccos(\omega) \in [0, \frac{\pi}{2}[,$$

where $a^{\alpha\beta}$ is the constant of proportionality appearing in the interaction potentiel, which is of the form $\Phi^{\alpha\beta}(r) = \frac{a^{\alpha\beta}}{4r^4}$ for Maxwellian molecules, with r denoting the distance between two particles, and g is a function depending on θ, implicitely defined by

$$\theta = \int_{y=0}^{y=y_c(g)} \frac{1}{\sqrt{(1 - (\frac{y}{g})^4 - y^2)}} \mathrm{d}y, \qquad y_c(g) = [\frac{-g^4 + (g^8 + 4g^4)^{\frac{1}{2}}}{2}]^{\frac{1}{2}}.$$

To ensure a definite value of $\nu^{\alpha\beta}$, it is necessary to perform a cut-off, i.e ignore the collisions with a incident angle $\theta \in [\theta_c, \frac{\pi}{2}]$, where θ_c is the so-called cut-off angle. Then, with this expression of $B^{\alpha\beta}(\theta)$, the following expressions hold $\forall \alpha, \beta$,

$$\nu^{\alpha\beta} = 2\pi (\frac{a^{\alpha\beta}}{\mu^{\alpha\beta}})^{\frac{1}{2}} g_c^{\alpha\beta}, \qquad \chi^{\alpha\beta} = 2\pi (\frac{a^{\alpha\beta}}{\mu^{\alpha\beta}})^{\frac{1}{2}} A(g_c^{\alpha\beta}),$$

where $g_c^{\alpha\beta} = g(\theta_c)$ depends only on the cut-off angle for $\alpha - \beta$ collisions, and A is a function defined by

$$A(z) = 2 \int_{g=0}^{g=z} g \cos^2(\theta) \mathrm{d}g.$$

Then, the dimensionless ratio are

$$\frac{\nu^{\alpha\beta}}{\nu^{11}} = (\frac{a^{\alpha\beta}}{a^{11}})^{\frac{1}{2}} \frac{m^1}{2} \frac{m^\alpha + m^\beta}{m^\alpha m^\beta} (\frac{g_c^{\alpha\beta}}{g_c^{11}})^2, \qquad \frac{\chi^{\alpha\beta}}{\nu^{11}} = \frac{\nu^{\alpha\beta}}{\nu^{11}} \frac{A(g_c^{\alpha\beta})}{(g_c^{\alpha\beta})^2}.$$

By assuming that $\forall \alpha, \beta, a^{\alpha\beta} = a^{11} = a$ and $g_c^{\alpha\beta} = g_c^{11} = g_c$, one gets the following expressions for $\nu^{\alpha\beta}$ and $\chi^{\alpha\beta}$:

$$\nu^{\alpha\beta} = \frac{m^1}{2} \frac{m^\alpha + m^\beta}{m^\alpha m^\beta} \nu^{11}, \qquad \chi^{\alpha\beta} = \nu^{\alpha\beta} \frac{A(g_c)}{g_c^2}.$$

Finally, it can be proven that $0 < \frac{A(z)}{z^2} \leq 1, \forall z$. Then, in this work, it is assumed that $\frac{A(g_c)}{(g_c)^2} = 1$, which amounts to $\chi^{\alpha\beta} = \nu^{\alpha\beta}$.

Performing a Champan-Enskog expansion from the present BGK model leads to a compressible Navier-Stokes system. The computations the mass flux J_i, of the stress tensor P and of the heat flux J_q coming from the model of Andries, Aoki and Perthame ([1]) leads to the following relations involving the transport coefficients

$$J^\alpha = -\sum_{\beta=1}^{N} L^{\alpha\beta} \frac{\nabla_x(n^\beta k_B T)}{\rho^\beta} \tag{8}$$

$$P = nk_BT \text{ Id } - \eta(\nabla_x u + (\nabla_x u)^t - \frac{2}{3}\nabla \cdot u) \tag{9}$$

$$J_q = \frac{5}{2}k_BT \sum_{\beta=1}^{N} \frac{J^\beta}{m^\beta} - \kappa \nabla T, \tag{10}$$

with

$$\eta = k_BT \sum_{\alpha=1}^{N} \frac{n^\alpha}{\nu^\alpha}, \quad \kappa = \frac{5}{2}k_B^2 T \sum_{\alpha=1}^{N} \frac{n^\alpha}{m^\alpha \nu^\alpha}.$$

η and κ represent respectively the viscosity and the thermal conductivity. The collision frequencies ν^α can be classically adjusted in order to fit the vicosity. But in that case the thermal conductivity coefficient is wrong. Moreover, according to ([15]), the expressions (8) and (10) give that the Soret and the Dufour coefficients are equal to 0. In the case of Maxwellian molecules, Soret and Duffour coefficients are effectively equal to 0. But, for more general potentials, this is wrong. Moreover, as explained in ([1]), the coefficents $L^{\alpha\beta}$ in 8 form a symmetric matrix depending only on masses and densities that is different from the matrix coming from the Boltzmann operator.

3. A local discrete velocity method

3.1. **Overview of the method.** The objective is to extend the method proposed in [10] to the case of multi-species rarefied flows. Locally in time and space, a distribution function is a function of microscopic velocity v, defined over all $\mathbb{R}$. For computational purposes, an adequate subset of $\mathbb{R}$ has to be chosen in order to encompass the distribution function correctly. For a given time t and point x, by assuming that the distribution function in v is Maxwellian, the quantities u and $\frac{k_BT}{m}$ correspond respectively to the expected value and the standard deviation of a Gaussian distribution. Hence, in usual methods, according to the confidence interval of Gaussian distributions, these quantities allow for the definition of a suitable velocity interval of the form $[V_{\min}, V_{\max}] \subset \mathbb{R}$, which is then replaced by a set of N_v discrete velocities to define a discrete velocity grid $\mathcal{V} = \{(v_k)_k, k \in \{1, ..., N_v\}\}$, which is uniform in space and time.

The idea developed in [10] consists in choosing local grids for every space discretization point, that depend on the local value of the macroscopic velocity and temperature, in the mono-species case. These grids are also chosen to be dynamic, i.e they depend on time by being recomputed at every time step, to account for the change of velocity and temperature.

By denoting with an index i and a superscript n the quantities computed at the point x_i and at time t^n, this method amounts to defining discrete velocity grids $\mathcal{V}_i^n = \{(v_{i,k}^n)_k, k \in \{1, ..., N_v\}\}$, which are now time and space dependant.

Firstly, this method prevents the use of a global grid that would be identical for all space points. The usual approach requires to choose a velocity grid that is large enough to encompass the largest distribution (i.e the distribution with the greatest temperature) and that is fine enough to properly capture the narrowest distribution. Necessarily, such a choice would have a high computational cost, with an important amount of unnecessary computations. Secondly, the local grids are recomputed at the beginning of every time step. Hence, this method also prevents the

need for a convergence test, that would be mandatory with static grids. More precisely, static grids require the initial (and only) choice for the velocity grid to be suitable even for subsequent times, where temperature could increase, for example. With dynamic grids, this is circumvented by the dependance on time.

For every time step, to compute $(f_{i,k}^{n+1})_k$, the method consists in the following steps:

(1) Computation of the velocity grid $\mathcal{V}_i^{n+1}, \forall i \in \{1, ..., N_x\}$
(2) Computation of the discrete Maxwellian distribution $(\overline{M}_{i,k}^{\alpha,n+1})_k$, defined by the macroscopic quantities computed in (1).
(3) Interpolation of the distributions $(f_{i,k}^n)_k$,$(f_{i-1,k}^n)_k$ and $(f_{i+1,k}^n)_k$ on the grid $\mathcal{V}_i^{n+1}$.
(4) Computation of f_i^{n+1} on the new grid, using an upwind scheme with an implicit relaxation term.
(5) Updating the macroscopic quantities of $(f_{i+1,k}^n)_k$ on the grid $\mathcal{V}_i^{n+1}$.

In this work, this procedure is extended to the case of multi-species flows. For species α, the quantities u^α and $\frac{T^\alpha}{m^\alpha}$ allow for the choice of the velocity grids. As can be seen, even with comparable velocities and temperatures, distributions may be different from one another because of the presence of m^α in the standard deviation. Hence, in this method, the grids will not only depend on space and time, but also on the considered species. This new method requires to define, for all i, n and α, discrete velocity grids of the form $\mathcal{V}_i^{\alpha,n} = \{(v_{i,k}^{\alpha,n})_k, k \in \{1, ..., (N_v)_i^{\alpha,n}\}\}$.

3.2. **Computation of the local velocity grids $\mathcal{V}_i^{\alpha,n}$.** Assume that quantities $(f_{i,k}^{\alpha,n})_k$ are known for all $i \in \{1, ..., N_x\}$ and $\alpha \in \{1, ..., N\}$. Define $(N_v)_i^{\alpha,n+1}$ the number of discrete velocities for species α at time t^{n+1} and point x_i. Step (1) of the method consists in defining the velocity grids:

(11)
$$\mathcal{V}_i^{\alpha,n+1} = \{(v_{i,k}^{\alpha,n+1})_k = (V_{\min})_i^{\alpha,n+1} + (k-1)\frac{(V_{\max})_i^{\alpha,n+1} - (V_{\min})_i^{\alpha,n+1}}{(N_v)_i^{\alpha,n+1} - 1}, k \in \{1, ..., (N_v)_i^{\alpha,n+1}\}\},$$

where $(V_{\min})_i^{\alpha,n+1}$ and $(V_{\max})_i^{\alpha,n+1}$ depend on space, time and species. In order to compute these intervals, it is then necessary to compute the adequate bounds of the discrete velocity grids $V_{\min}$ and $V_{\max}$.

These bounds are given by the following formula, for every i, α:

$$[(V_{\min})_i^{\alpha,n+1}, (V_{\max})_i^{\alpha,n+1}] = [u_i^{\alpha,n+1} - l_i^\alpha\sqrt{\frac{k_B T_i^{\alpha,n+1}}{m^\alpha}}, u_i^{\alpha,n+1} + l_i^\alpha\sqrt{\frac{k_B T_i^{\alpha,n+1}}{m^\alpha}}], \tag{12}$$

where l^α is an integer that can be tweaked to fit the flow regime under consideration. In the case of Euler flows, where the distribution is assumed to be Maxwellian, the confidence interval of a Gaussian distribution gives $l_i^\alpha = 4$, which gives a lower bound for this value.

According to (12), the computation of the velocity grids requires the knowledge of $u_i^{\alpha,n+1}$ and $T_i^{\alpha,n+1}$. Moreover, the knowledge of these quantities allows for the computation of the Maxwellian $(\overline{M}_{i,k}^{\alpha,n+1})_k$, which enables the implicit treatment of the BGK operator in the discrete equations (more details are given in the next section). In order to obtain equations on these quantities, consider the following semi-discretization of equation (3) (variable v is kept continuous):

$$f_i^{\alpha,n+1}(v) = f_i^{\alpha,n}(v) - \frac{\Delta t}{\Delta x}(\phi_{i+\frac{1}{2}}^{\alpha,n}(v) - \phi_{i-\frac{1}{2}}^{\alpha,n}(v)) + \Delta t \nu_i^{\alpha,n+1}(\overline{M}_i^{\alpha,n+1}(v) - f_i^{\alpha,n+1}(v)), \tag{13}$$

where

$$\phi_{i+\frac{1}{2}}^{\alpha,n}(v) = \frac{1}{2}\left(v\left(f_{i+1}^{\alpha,n}(v) + f_i^{\alpha,n}(v)\right) - |v|\left(f_{i+1}^{\alpha,n}(v) - f_i^{\alpha,n}(v)\right)\right),$$

is the classical upwind discretization of the flux. Note that the implicitation of the relaxation operator allows for a scheme that is inconditionnaly stable regarding the relaxation frequency. Then, the scheme is asymptotic-preserving in the limit $\nu^\alpha \to +\infty$, which gives a kinetic scheme for Euler.

By writing conservation laws, velocities and temperatures can be computed by solving linear systems. For the velocities, the following proposition holds:

Proposition 1. *For every point x_i of the physical domain, i.e. $\forall i \in \{1, ..., N_x\}$, velocities $(u_i^{\alpha,n+1})_\alpha$ solve the following $N \times N$ linear system:*

$$A_i U_i^{n+1} = B_i, \tag{14}$$

where

$$U_i^{n+1} = (u_i^{1,n+1}, ..., u_i^{N,n+1})^T, \qquad B_i^\alpha = \rho_i^{\alpha,n} u_i^{\alpha,n} - \frac{\Delta t}{\Delta x} \langle m^\alpha v (\phi_{i+\frac{1}{2}}^{\alpha,n} - \phi_{i-\frac{1}{2}}^{\alpha,n}) \rangle,$$

and for all $\alpha \in \{1, ..., N\}$ and $\beta \neq \alpha$, the elements of the matrices A_i read:

$$(A_i)_{\alpha\alpha} = \rho_i^{\alpha,n+1} + 2\Delta t n_i^{\alpha,n+1} \sum_{\substack{\beta=1 \\ \beta\neq\alpha}}^{N} \mu^{\alpha\beta} \chi^{\alpha\beta} n_i^{\beta,n+1},$$

$$(A_i)_{\alpha\beta} = -2\Delta t n_i^{\alpha,n+1} \mu^{\alpha\beta} \chi^{\alpha\beta} n_i^{\beta,n+1}.$$

Under the assumption of non-vacuum solutions ($\rho_i^{\alpha,n} > 0$), each system (14) admits a unique solution.

Proof. By integrating this equation over v (i.e taking the 0^{th}-order moment), concentrations at time t^{n+1} can be computed, $\forall i \in \{1, ..., N_x\}$ and $\alpha \in \{1, ..., N\}$:

$$n_i^{\alpha,n+1} = n_i^{\alpha,n} - \frac{\Delta t}{\Delta x} \langle \phi_{i+\frac{1}{2}}^{\alpha,n} - \phi_{i-\frac{1}{2}}^{\alpha,n} \rangle.$$

Then, $\nu^{\alpha,n+1} = \sum_{\beta=1}^{N} \nu^{\alpha\beta} n^{\beta,n+1}$ can be computed. To obtain equations on the velocities, take the first-order moment of equation (13), one obtains:

$$\rho_i^{\alpha,n+1} u_i^{\alpha,n+1} = \rho_i^{\alpha,n} u_i^{\alpha,n} - \frac{\Delta t}{\Delta x} \langle m^\alpha v (\phi_{i+\frac{1}{2}}^{\alpha,n} - \phi_{i-\frac{1}{2}}^{\alpha,n}) \rangle + \Delta t \nu_i^{\alpha,n+1} \rho_i^{\alpha,n+1} (\overline{u}_i^{\alpha,n+1} - u_i^{\alpha,n+1}).$$

By using the definition of mixture velocities (6), this leads to:

$$\begin{aligned} \rho_i^{\alpha,n+1} u_i^{\alpha,n+1} = \rho_i^{\alpha,n} u_i^{\alpha,n} &- \frac{\Delta t}{\Delta x} \langle m^\alpha v (\phi_{i+\frac{1}{2}}^{\alpha,n} - \phi_{i-\frac{1}{2}}^{\alpha,n}) \rangle \\ &+ 2\Delta t n_i^{\alpha,n+1} \sum_{\beta=1}^{N} \mu^{\alpha\beta} \chi^{\alpha\beta} n_i^{\beta,n+1} (u_i^{\beta,n+1} - u_i^{\alpha,n+1}). \end{aligned}$$

Finally, for all α, i:

$$\begin{aligned} \left(\rho_i^{\alpha,n+1} + 2\Delta t n_i^{\alpha,n+1} \sum_{\substack{\beta=1 \\ \beta\neq\alpha}}^{N} \mu^{\alpha\beta} \chi^{\alpha\beta} n_i^{\beta,n+1} \right) u_i^{\alpha,n+1} &- 2\Delta t n_i^{\alpha,n+1} \sum_{\substack{\beta=1 \\ \beta\neq\alpha}}^{N} \mu^{\alpha\beta} \chi^{\alpha\beta} n_i^{\beta,n+1} u_i^{\beta,n+1} \\ &= \rho_i^{\alpha,n} u_i^{\alpha,n} - \frac{\Delta t}{\Delta x} \langle m^\alpha v (\phi_{i+\frac{1}{2}}^{\alpha,n} - \phi_{i-\frac{1}{2}}^{\alpha,n}) \rangle. \end{aligned}$$

These equations can be put under the form (14).

For all i, the matrix A_i is strictly diagonally dominant (by assumption of non-vacuum solutions, i.e $\rho_i^{\alpha,n} > 0$). Then, in favor of Gershgorin's theorem, A_i is invertible and the system possess a unique solution. □

Solving these systems allows for the computation of the values of partial velocities $u_i^{\alpha,n+1}$, which in turn allows for the computation of mixture velocities $\overline{u}_i^{\alpha,n+1}$ (in favor of (6)). By assuming these quantities to be known, a similar procedure can be applied in order to compute internal energies $\varepsilon_i^{\alpha,n+1}$, which then allows for the computation of the temperatures $T_i^{\alpha,n+1}$ and

mixture temperatures $\overline{T}_i^{\alpha,n+1}$, according to (7). The procedure is summed up in the following proposition:

Proposition 2. *For every space point x_i, i.e $\forall i \in \{1, ..., N_x\}$, internal energies $(\varepsilon_i^{\alpha,n+1})_\alpha$ solve the following $N \times N$ linear system:*

$$G_i Y_i^{n+1} = C_i, \tag{15}$$

where $Y_i^{n+1} = (\varepsilon_i^1, ..., \varepsilon_i^N)^T$ is the vector of all internal energies at point x_i. Moreover, $C_i \in \mathbb{R}^N$ and the component α of C_i is given by:

$$\begin{aligned}
C_i^\alpha = E_i^{\alpha,n} &- \frac{\Delta t}{\Delta x}\langle m^\alpha \frac{v^2}{2}(\phi_{i+\frac{1}{2}}^{\alpha,n} - \phi_{i-\frac{1}{2}}^{\alpha,n})\rangle \\
&- \frac{1}{2}m^\alpha n_i^{\alpha,n+1}(u_i^{\alpha,n+1})^2 + \Delta t \nu_i^{\alpha,n+1}\frac{m^\alpha}{2}n_i^{\alpha,n+1}((\overline{u}_i^{\alpha,n+1})^2 - (u_i^{\alpha,n+1})^2) \\
&- \Delta t n_i^{\alpha,n+1}\frac{m^\alpha \nu_i^{\alpha,n+1}}{2}(\overline{u}_i^{\alpha,n+1} - u_i^{\alpha,n+1})^2 \\
&+ \Delta t n_i^{\alpha,n+1}\sum_{\substack{\beta=1 \\ \beta\neq\alpha}}^{N} \mu^{\alpha\beta}\chi^{\alpha\beta}n_i^{\beta,n+1}\frac{4}{m^\alpha + m^\beta}(m^\beta \frac{(u_i^{\beta,n+1} - u_i^{\alpha,n+1})^2}{2}),
\end{aligned}$$

where $E_i^{\alpha,n}$ denotes the total energy of species α at time t^n and point x_i. Finally, the matrix $G_i \in \mathcal{M}_{N\times N}(\mathbb{R})$ is given by

$$\begin{aligned}
(G_i)_{\alpha\alpha} &= n_i^{\alpha,n+1} + \Delta t n_i^{\alpha,n+1}\sum_{\substack{\beta=1 \\ \beta\neq\alpha}}^{N} \mu^{\alpha\beta}\chi^{\alpha\beta}n_i^{\beta,n+1}\frac{4}{m^\alpha + m^\beta}, \\
(G_i)_{\alpha\beta} &= -\Delta t n_i^{\alpha,n+1}\mu^{\alpha\beta}\chi^{\alpha\beta}n_i^{\beta,n+1}\frac{4}{m^\alpha + m^\beta}.
\end{aligned}$$

Proof. Take the second-order moment of equation (13).

$$\begin{aligned}
\frac{1}{2}m^\alpha n_i^{\alpha,n+1}(u_i^{\alpha,n+1})^2 + n_i^{\alpha,n+1}\varepsilon_i^{\alpha,n+1} = E_i^{\alpha,n} &- \frac{\Delta t}{\Delta x}\langle m^\alpha \frac{v^2}{2}(\phi_{i+\frac{1}{2}}^{\alpha,n} - \phi_{i-\frac{1}{2}}^{\alpha,n})\rangle \\
&+ \Delta t \nu_i^{\alpha,n+1}(\overline{E}_i^{\alpha,n+1} - E_i^{\alpha,n+1}).
\end{aligned}$$

According to the definition of mixture energies (7), it comes

$$\begin{aligned}
n_i^{\alpha,n+1}\varepsilon_i^{\alpha,n+1} = E_i^{\alpha,n} &- \frac{\Delta t}{\Delta x}\langle m^\alpha \frac{v^2}{2}(\phi_{i+\frac{1}{2}}^{\alpha,n} - \phi_{i-\frac{1}{2}}^{\alpha,n})\rangle \\
&- \frac{1}{2}m^\alpha n_i^{\alpha,n+1}(u_i^{\alpha,n+1})^2 + \Delta t \nu_i^{\alpha,n+1}\frac{m^\alpha}{2}n_i^{\alpha,n+1}((\overline{u}_i^{\alpha,n+1})^2 - (u_i^{\alpha,n+1})^2) \\
&- \Delta t n_i^{\alpha,n+1}\frac{m^\alpha \nu_i^{\alpha,n+1}}{2}(\overline{u}_i^{\alpha,n+1} - u_i^{\alpha,n+1})^2 \\
&+ \Delta t n_i^{\alpha,n+1}\sum_{\substack{\beta=1 \\ \beta\neq\alpha}}^{N} \mu^{\alpha\beta}\chi^{\alpha\beta}\frac{4n_i^{\beta,n+1}}{m^\alpha + m^\beta}(\varepsilon_i^{\beta,n+1} - \varepsilon_i^{\alpha,n+1} + m^\beta \frac{(u_i^{\beta,n+1} - u_i^{\alpha,n+1})^2}{2}).
\end{aligned}$$

Then, by rearranging the terms, one gets the following equations on internal energies:

$$
\begin{aligned}
&(n_i^{\alpha,n+1} + \Delta t n_i^{\alpha,n+1} \sum_{\substack{\beta=1\\ \beta\neq\alpha}}^{N} \mu^{\alpha\beta}\chi^{\alpha\beta}\frac{4n_i^{\beta,n+1}}{m^\alpha+m^\beta})\varepsilon_i^{\alpha,n+1} - \Delta t n_i^{\alpha,n+1}\sum_{\substack{\beta=1\\ \beta\neq\alpha}}^{N}\mu^{\alpha\beta}\chi^{\alpha\beta}\frac{4n_i^{\beta,n+1}}{m^\alpha+m^\beta})\varepsilon_i^{\beta,n+1}\\
&\quad = E_i^{\alpha,n} - \frac{\Delta t}{\Delta x}\langle m^\alpha\frac{v^2}{2}(\phi_{i+\frac12}^{\alpha,n} - \phi_{i-\frac12}^{\alpha,n})\rangle - \frac{m^\alpha}{2}n_i^{\alpha,n+1}(u_i^{\alpha,n+1})^2\\
&\quad + \Delta t\nu_i^{\alpha,n+1}\frac{m^\alpha}{2}n_i^{\alpha,n+1}((\overline{u}_i^{\alpha,n+1})^2 - (u_i^{\alpha,n+1})^2)\\
&\quad - \Delta t n_i^{\alpha,n+1}\frac{m^\alpha\nu_i^{\alpha,n+1}}{2}(\overline{u}_i^{\alpha,n+1} - u_i^{\alpha,n+1})^2\\
&\quad + \Delta t n_i^{\alpha,n+1}\sum_{\substack{\beta=1\\ \beta\neq\alpha}}^{N}\mu^{\alpha\beta}\chi^{\alpha\beta}\frac{4n_i^{\beta,n+1}}{m^\alpha+m^\beta}\frac{m^\beta}{2}(u_i^{\beta,n+1} - u_i^{\alpha,n+1})^2.
\end{aligned}
$$

These equations can then be put in form (15). Under the same argument as previously, existence and uniqueness of solutions are ensured. □

Numerically, all integrals with respect to v are approximated by a trapezoidal quadrature formula, according to

$$\langle f^\alpha(t^n, x_i, v)\rangle = \sum_{k=1}^{N_v} f^\alpha(t^n, x_i, v_k)\omega_k\Delta v_{i,k}^{\alpha,n},$$

where $\omega_1 = \omega_{N_v} = \frac12$ and $\omega_k = 1$ for $k = \{2, ..., N_v - 1\}$.

Grid bounds are then computed according to formula (12), and the discrete velocities are given by

$$v_{i,k}^{\alpha,n+1} = (V_{\min})_i^{\alpha,n+1} + (k-1)\frac{(V_{\max})_i^{\alpha,n+1} - (V_{\min})_i^{\alpha,n+1}}{(N_v)_i^{\alpha,n+1} - 1}, \qquad \forall k \in \{1, ..., (N_v)_i^{\alpha,n+1}\},$$

for all i and α.

3.3. **Interpolation and computation of the distribution functions.** Consider now the discretization of equation (13) on grids $\mathcal{V}_i^{\alpha,n+1}$. It reads:

$$f_{i,k}^{\alpha,n+1} = \tilde{f}_{i,k}^{\alpha,n} - \frac{\Delta t}{\Delta x}(\tilde{\phi}_{i+\frac12,k}^{\alpha,n} - \tilde{\phi}_{i-\frac12,k}^{\alpha,n}) + \Delta t\nu_i^{\alpha,n+1}(\overline{M}_{i,k}^{\alpha,n+1} - f_{i,k}^{\alpha,n+1}),$$

which gives the following update formula:

$$f_{i,k}^{\alpha,n+1} = \frac{1}{1+\Delta t\nu_i^{\alpha,n+1}}\left(\tilde{f}_{i,k}^{\alpha,n} - \frac{\Delta t}{\Delta x}(\tilde{\phi}_{i+\frac12,k}^{\alpha,n} - \tilde{\phi}_{i-\frac12,k}^{\alpha,n}) + \Delta t\nu^{\alpha,n+1}\overline{M}_{i,k}^{\alpha,n+1}\right),$$

where $\tilde{f}_{i,k}^{\alpha,n}, \tilde{\phi}_{i+\frac12,k}^{\alpha,n}, \tilde{\phi}_{i-\frac12,k}^{\alpha,n}$ denotes the interpolation of the quantities $f_{i,k}^{\alpha,n}, \phi_{i+\frac12,k}^{\alpha,n}, \phi_{i-\frac12,k}^{\alpha,n}$ on the newly-defined grid $\mathcal{V}_i^{\alpha,n+1}$. This interpolation step is necessary because quantities are all defined on different velocity grids. More precisely, for every point in space x_i, the quantities constituting the stencil of the upwind scheme are interpolated. Hence, for fixed α and i, and for $p \in \{i-1, i, i+1\}$, and for all $v \in \mathcal{V}_i^{\alpha,n+1}$, the quantities $f^\alpha(t^n, x_p, v)$ are interpolated.

To do so, an ENO4 (Essentially Non-Oscillatory with 4 points) interpolation procedure is applied. This method has been developped by Harten in [20] (a excellent presentation can be found in [31]).

Let us give an overview of the method. Consider for example the set $(f_{i,k}^{\alpha,n})_k$ that is defined on the grid $\mathcal{V}_i^{\alpha,n}$. The objective is to interpolate it on the grid $\mathcal{V}_i^{\alpha,n+1}$. For each velocity $v_{i,k}^{\alpha,n+1} \in \mathcal{V}_i^{\alpha,n+1}$, the first step consists in finding the index l such that

$$v_{i,k}^{\alpha,n+1} \in]v_{i,l}^{\alpha,n}, v_{i,l+1}^{\alpha,n}[,$$

where the case where $v_{i,k}^{\alpha,n+1}$ is out of the bounds of the grid has been dismissed. In this case, since we are working with distribution functions that are assumed to be compactly supported on these intervals, the interpolated value is set to zero.

Once the velocity $v_{i,k}^{\alpha,n+1}$ has been pinpointed, the method consists in finding the best 4-point stencil to interpolate the values. "Best" means here that it is necessary to avoid interpolating with values across a discontinuity, for example. Hence, the procedure consists in taking the two-point stencil $\{v_{i,l}^{\alpha,n}, v_{i,l+1}^{\alpha,n}\}$ and adding a third point, either $v_{i,l-1}^{\alpha,n}$ or $v_{i,l+2}^{\alpha,n}$, by taking the point that give the smallest divided difference. Then, without loss of generality, assume that $v_{i,l-1}^{\alpha,n}$ has been chosen. The last point of the stencil is then chosen between $v_{i,l-2}^{\alpha,n}$ and $v_{i,l+2}^{\alpha,n}$ in a similar fashion.

According to the previous section, partial and mixture quantities at time t^{n+1} are known. Hence, $\overline{M}_{i,k}^{\alpha,n+1}$ is known for all α, i and k.

3.4. **Grid enlargement.** In this section, an optional improvement of the method is presented. It consists in enabling the method to adapt to the level of rarefaction of the gas. More precisely, in the method developed so far, the quantities l^α are set ad hoc at the beginning of the computation. Choosing $l^\alpha = 4$ or 5 works perfectly when distributions are not too far from Maxwellian equilibrium, as can be seen on the test cases in section 5. However, when the flow is rarefied, there might be a need for a convergence test even with the adaptive methods.

The extension proposed here consists in splitting the transport and relaxation parts of the equations. At each space point, once the transport step is performed, the ratio between the maximum value of the distribution and the value on the left bound of the velocity domain is computed.

$$\mathcal{R} = \frac{f_{i,1}^{\alpha,n+1}}{\max_k (f_{i,k}^{\alpha,n+1})}.$$

If this ratio is greater than a prescribed tolerance (when this method has been used in practice, the tolerance has been chosen equal to 10^{-6}), a discrete velocity is added at the left of the grid, and the transport step is performed again. This procedure is then repeated until the requirement on the ratio is met. Then, the method is applied to the right bound of the domain, where the ratio requirement writes as:

$$\mathcal{R} = \frac{f_{i,N_v}^{\alpha,n+1}}{\max_k (f_{i,k}^{\alpha,n+1})}.$$

This method will be employed for the heat transfer test cases in the next section, which are considered in rarefied regimes.

4. Extension of the method: shifted velocity grids

The method presented in the previous section necessitates, for all i and α, the interpolation of the three distribution functions $f_i^{\alpha,n}(v), f_{i-1}^{\alpha,n}(v)$ and $f_{i+1}^{\alpha,n}(v)$ on each point $v_{i,k}^{\alpha,n+1}$, for all k. Compared to the usual static grid method, this significant amount of computations increases the computational cost and degrade the accuracy of the numerical solutions. In order to reduce the number of interpolations, the local velocity grid method presented above can be improved in the following manner. Once grids at time t^{n+1} are computed by the procedure explained in section 3.2, they are slightly shifted in order to have the maximum number of shared velocities between each grid, so that all the corresponding interpolations will become unnecessary, as the distribution functions will already be known at these points. Of course, if two adjacent velocity grids are different, the interpolation procedure is mandatory. This goal of this method is to diminish the number of interpolations. But it is not possible to avoid them totally.

4.1. **Notations and computation of the initial bounds and steps.** Firstly, consider the initialization of the local velocity grids. For given initial conditions $n_i^{\alpha,0}, u_i^{\alpha,0}, T_i^{\alpha,0}$ and a given reference number of discrete velocities N_v, every grid $\mathcal{V}_i^{\alpha,0}$ is computed according to formula (12). Then, in order to shift them, denote the smallest velocity step for every species:

$$\Delta v_{\min}^{\alpha,0} = \min_i (\Delta v_i^{\alpha,0}). \tag{16}$$

Then, the value of all the other velocities steps are adjusted in order to be equal to the nearest multiple of $\Delta v_{\min}^{\alpha}$. The corrected value is then denoted with an overline:

$$\overline{\Delta v}_i^{\alpha} = \lfloor \frac{\Delta v_i^{\alpha}}{\Delta v_{\min}^{\alpha,0}} \rceil \Delta v_{\min}^{\alpha,0}, \tag{17}$$

where $\lfloor x \rceil$ denotes the nearest integer to x. Subsequently, it is necessary to modify the bounds of the interval in a similar fashion: the lower bound $(V_{\min})_i^{\alpha,0}$ is shifted to the greatest multiple of $\overline{\Delta v}_i^{\alpha,0}$ that is smaller than $(V_{\min})_i^{\alpha,0}$. Similarly, the upper bound $(V_{\max})_i^{\alpha,0}$ is shifted to the lowest multiple of $\overline{\Delta v}_i^{\alpha,0}$ that is greater than $(V_{\max})_i^{\alpha,0}$. The updated values read:

$$(\overline{V_{\min}})_i^{\alpha,0} = \lfloor \frac{(V_{\min})_i^{\alpha,0}}{\overline{\Delta v}_i^{\alpha,0}} \rfloor \overline{\Delta v}_i^{\alpha,0}, \qquad (\overline{V_{\max}})_i^{\alpha,0} = \lceil \frac{(V_{\max})_i^{\alpha,0}}{\overline{\Delta v}_i^{\alpha,0}} \rceil \overline{\Delta v}_i^{\alpha,0}, \tag{18}$$

where $\lfloor x \rfloor$ and $\lceil x \rceil$ denote respectively the integer part of x and the integer part of $x+1$. This procedure ensures that, for fixed α, all quantities $(\overline{V_{\min}})_i^{\alpha,0}, (\overline{V_{\max}})_i^{\alpha,0}$ and $\overline{\Delta v}_i^{\alpha}$ are multiples in $\mathbb{Z}$ of $\Delta v_{\min}^{\alpha,0}$.

4.2. **Computation of the initial shifted grids.** Finally, the new shifted grids can be computed. Since the bounds and the steps have been modified, the number of discrete velocities for each grid may also be increased. However, it will be shown that the quantity of added velocities stay relatively small. The new amount of discrete velocities at point x_i for species α, denoted $(\overline{N_v})_i^{\alpha,0}$ is given by

$$(\overline{N_v})_i^{\alpha,0} = \frac{(V_{\max})_i^{\alpha,0} - (V_{\min})_i^{\alpha,0}}{\overline{\Delta v}_i^{\alpha,0}} - 1. \tag{19}$$

Then, according to formula (11), the shifted grids are obtained as:

$$\mathcal{V}_i^{\alpha,0} = \{(v_{i,k}^{\alpha,0})_k = (\overline{V_{\min}})_i^{\alpha,0} + (k-1)\frac{(\overline{V_{\max}})_i^{\alpha,0} - (\overline{V_{\min}})_i^{\alpha,0}}{(\overline{N_v})_i^{\alpha,0} - 1}, k \in \{1, ..., (\overline{N_v})_i^{\alpha,0}\}\}. \tag{20}$$

4.3. **Computation of subsequent shifted grids.** For subsequent times, the procedure (16)-(17)-(18)-(19)-(20) is applied in order to obtain bounds and steps at time t^{n+1} that are multiples of the same quantity. However, it is now necessary to also ensure that the grids will be homothetic to the grids at time t^n. To that end, once (16) is performed, two cases can occur. The first one is the following:

$$\Delta v_{\min}^{\alpha,n+1} \geq \Delta v_{\min}^{\alpha,n}.$$

In this case, $\Delta v_{\min}^{\alpha,n+1}$ is set equal to its nearest multiple of $\Delta v_{\min}^{\alpha,n}$, given by:

$$(\overline{\Delta v_{\min}})_i^{\alpha,n+1} = \lfloor \frac{(\Delta v_{\min})_i^{\alpha,n+1}}{\Delta v_{\min}^{\alpha,n}} \rceil \Delta v_{\min}^{\alpha,n}.$$

Hence, discrete velocities at time t^{n+1} will be multiples of $\Delta v_{\min}^{\alpha,n}$. The second case is:

$$\Delta v_{\min}^{\alpha,n+1} \leq \Delta v_{\min}^{\alpha,n}.$$

In this case, $\Delta v_{\min}^{\alpha,n+1}$ is modified in order to be equal to its nearest divider of $\Delta v_{\min}^{\alpha,n}$ which is given by:

$$(\overline{\Delta v_{\min}})_i^{\alpha,n+1} = \frac{1}{\lfloor \frac{(\Delta v_{\min})_i^{\alpha,n+1}}{\Delta v_{\min}^{\alpha,n}} \rceil} \Delta v_{\min}^{\alpha,n}.$$

This ensures that all discrete velocities at time t^n and t^{n+1} are multiples of $(\overline{\Delta v_{\min}})_i^{\alpha,n+1}$. Once this adjustment of $(\overline{\Delta v_{\min}})_i^{\alpha,n+1}$ is made, the remainder of the procedure (17)-(18)-(19)-(20) can be applied as previously.

The following proposition, concerning the increase of the number of discrete velocities after shifting the grids, can be stated.

Proposition 3. *The number of discrete velocities at point x_i for species α at time t^n after shifting $(\overline{N_v})_i^{\alpha,n}$ can be expressed in terms of the number of discrete velocities before shifting $(N_v)_i^{\alpha,n}$:*

$$(\overline{N_v})_i^{\alpha,n} = \frac{((N_v)_i^{\alpha,n}+1)(k_i^{\alpha,n}+s_i^{\alpha,n})}{k_i^{\alpha,n}+\lfloor s_i^{\alpha,n}\rceil} - 1 + R_i^{\alpha,n}, \tag{21}$$

where $R_i^{\alpha,n} \in [0,2[$ and $k_i^{\alpha,n} \in \mathbb{N}^*, s_i^{\alpha,n} \in [0,1[$ are defined as

$$\Delta v_i^{\alpha,n} = (k_i^{\alpha,n}+s_i^{\alpha,n})\Delta v_{min}^{\alpha,n}, \tag{22}$$

which can be equivalently defined as

$$k_i^{\alpha,n} = \lfloor \frac{\Delta v_i^{\alpha,n}}{\Delta v_{min}^{\alpha,n}} \rfloor, \qquad s_i^{\alpha,n} = \frac{\Delta v_i^{\alpha,n}}{\Delta v_{min}^{\alpha,n}} - \lfloor \frac{\Delta v_i^{\alpha,n}}{\Delta v_{min}^{\alpha,n}} \rfloor.$$

Proof. According to equations (22) and (17), it comes:

$$(\overline{\Delta v})_i^{\alpha,n} = (k_i^{\alpha,n} + \lfloor s_i^{\alpha,n} \rceil)\Delta v_{\min}^{\alpha,n}.$$

Then, according to (18), the velocity interval after shifting is slighty longer than the interval before. However, it exists $R_i^{\alpha,n} \in [0,2[$ such that:

$$(\overline{V_{\max}})_i^{\alpha,n} - (\overline{V_{\min}})_i^{\alpha,n} = (V_{\max})_i^{\alpha,n} - (V_{\min})_i^{\alpha,0} + R_i^{\alpha,n}\overline{\Delta v}_i^{\alpha,n} \tag{23}$$

This simply expresses that, in order to obtain bounds that are multiples of $(\overline{\Delta v})_i^{\alpha,n}$, they are at most increased by a quantity strictly inferior to $2(\overline{\Delta v})_i^{\alpha,n}$. Now, according to the definitions of N_v and $(\overline{N_v})_i^{\alpha,n}$, one gets:

$$(\overline{V_{\max}})_i^{\alpha,n} - (\overline{V_{\min}})_i^{\alpha,n} = ((\overline{N_v})_i^{\alpha,n}+1)(\overline{\Delta v})_i^{\alpha,n},$$
$$(V_{\max})_i^{\alpha,n} - (V_{\min})_i^{\alpha,n} = (N_v+1)(\Delta v)_i^{\alpha,n}.$$

By injecting these equations in (23), the following relation is obtained:

$$((\overline{N_v})_i^{\alpha,n}+1)(\overline{\Delta v})_i^{\alpha,n} = (N_v+1)(\Delta v)_i^{\alpha,n} + R_i^{\alpha,n}\overline{\Delta v}_i^{\alpha,n},$$

which then, in favor of (22) and (4.3), leads to:

$$((\overline{N_v})_i^{\alpha,n} + 1 - R_i^{\alpha,n})(k_i^{\alpha,n} + \lfloor s_i^{\alpha,n} \rceil)\Delta v_{\min}^{\alpha,n} = (N_v+1)(k_i^{\alpha,n} + \lfloor s_i^{\alpha,n} \rceil)\Delta v_{\min}^{\alpha,n}.$$

Finally, by simplifying by $\Delta v_{\min}^{\alpha,n}$ and rearranging the terms, one gets (21). □

A rough estimation of formula (21) gives that, even in the worst case where $\Delta v_i^{\alpha,n} = \frac{3}{2}\Delta v_{\min}^{\alpha,n}$, the increase in the number of discrete velocities will never exceed 50 percent. However, as will be seen in the numerical tests, depending on the test case, the increase in computation time due to this increase of discrete velocity may counterbalance the gain from interpolation decrease.

5. Numerical results

In this section, several test cases are presented in order to exhibit the behaviour of the method. It is compared with the results obtained with the classical static grids method. As stated before, this classical method needs a velocity grid that is large enough to contain the widest distribution and that is accurate enough to describe the most narrow one. Moreover, the grid being static in time, it needs to be suitable for any subsequent simulation time. The objective is to show that, for a chosen set of discretization parameters, the local grids method works better, and that the static grid methods needs a more important quantity of discrete velocities and larger bounds. To set notations, adaptive methods will be denoted LDV (Local Discrete Velocities), SLDV (Shifted

	l	N_v	CPU time
LDV	5	10	96,2s
SLDV	4	7	77,4s
DVM	5	30	86,7s

TABLE 1. Discrete parameters and computation time for test case 5.1

Local Discrete Velocities) and the standard method will be denoted DVM (Discrete Velocity Method). Two major parameters will be used to discriminate the different methods: the number of discrete velocities N_v and the length of the velocity grid (l^α in (12)).

In all the following experiments, the Boltzmann constant will be denoted k_B and will be equal to $1,38065.10^{-23}$ J.K^{-1}. Moreover, in all tests, $L_{\min} = 0$ and $L_{\max} = 1$ m and the domain is discretized with $N_x = 5000$ points, unless specified otherwise. Moreover, in all the following test cases, the number of species will be set to $N = 2$, but the method works for any number of components, and no stiffness appears in the method as N increases.

5.1. **A first Riemann problem.** The first test case is a Riemann problem, considered here for a gas composed of 2 species of respective particle mass $m^1 = 66,3.10^{-27}$ kg and $m^2 = 66,3.10^{-28}$ kg, which gives a mass ratio of 10. It consists in an initial discontinuity in velocity and temperature, given by the following data:

$$\begin{cases} u^1(t_0,x) = u^2(t_0,x) = 213,92 \text{ m.s}^{-1}, \text{ if } x \in [0,0.5], \\ u^1(t_0,x) = u^2(t_0,x) = -213,92 \text{ m.s}^{-1}, \text{ if } x \in [0.5,1], \end{cases}$$

and

$$\begin{cases} T^1(t_0,x) = 300 \text{ K }, T^2(t_0,x) = 600 \text{ K }, \text{ if } x \in [0,0.5], \\ T^1(t_0,x) = 500 \text{ K }, T^2(t_0,x) = 900 \text{ K }, \text{ if } x \in [0.5,1], \end{cases}$$

and densities are initially all equal to 1 kg.m^{-3} over the whole domain. The solution is computed at time $T = 10^{-4}$ s. The Knudsen number is chosen equal to 10^{-3}, which is a slightly rarefied regime. Parameters N_v and l, as well as the CPU time, are compiled in table 1. The results are displayed in figure 1.

The LDV method can be seen to be very effective with a very small number of discrete velocities ($N_v = 10$) and a standard grid length ($l^\alpha = 5$). The SLDV method gives results that are superimposed with the LDV method for an even smaller number of points ($N_v = 7$) and a shorter grid ($l^\alpha = 4$). On the other hand, the DVM method needs a longer domain ($l^\alpha = 6$) and more discrete velocities ($N_v = 100$). Otherwise, when used with the same velocity grids as for the SLDV method, as can be seen on the results for velocities and temperatures specifically, macroscopic quantities are not well computed.

Concerning computation time, the LDV method can be seen to actually be longer than the classical DVM method, but the gain in interpolation and the ability to reduce the initial number of discrete velocities allow the SLDV method to be the fastest method.

5.2. **Blast waves.** The second test case is a 2-species blast waves case, with respective particle mass $m^1 = 66,3.10^{-27}$ kg and $m^2 = 20 \times m^1 = 13,26.10^{-25}$ kg. It consists in two important discontinuities in temperature, given by the following data:

$$\begin{cases} \rho^1(t_0,x) = \rho^2(t_0,x) = 1 \text{ kg.m}^{-3}, & \forall x \in [0,1], \\ u^1(t_0,x) = u^2(t_0,x) = 0 \text{ m.s}^{-1}, & \forall x \in [0,1], \\ T^1(t_0,x) = T^2(t_0,x) = 4.8 \text{ K }, & \text{if } x \in [0,0.1], \\ T^1(t_0,x) = T^2(t_0,x) = 4.8.10^{-5} \text{ K }, & \text{if } x \in [0.1,0.9], \\ T^1(t_0,x) = T^2(t_0,x) = 4.8.10^{-1} \text{ K }, & \text{if } x \in [0.9,1]. \end{cases}$$

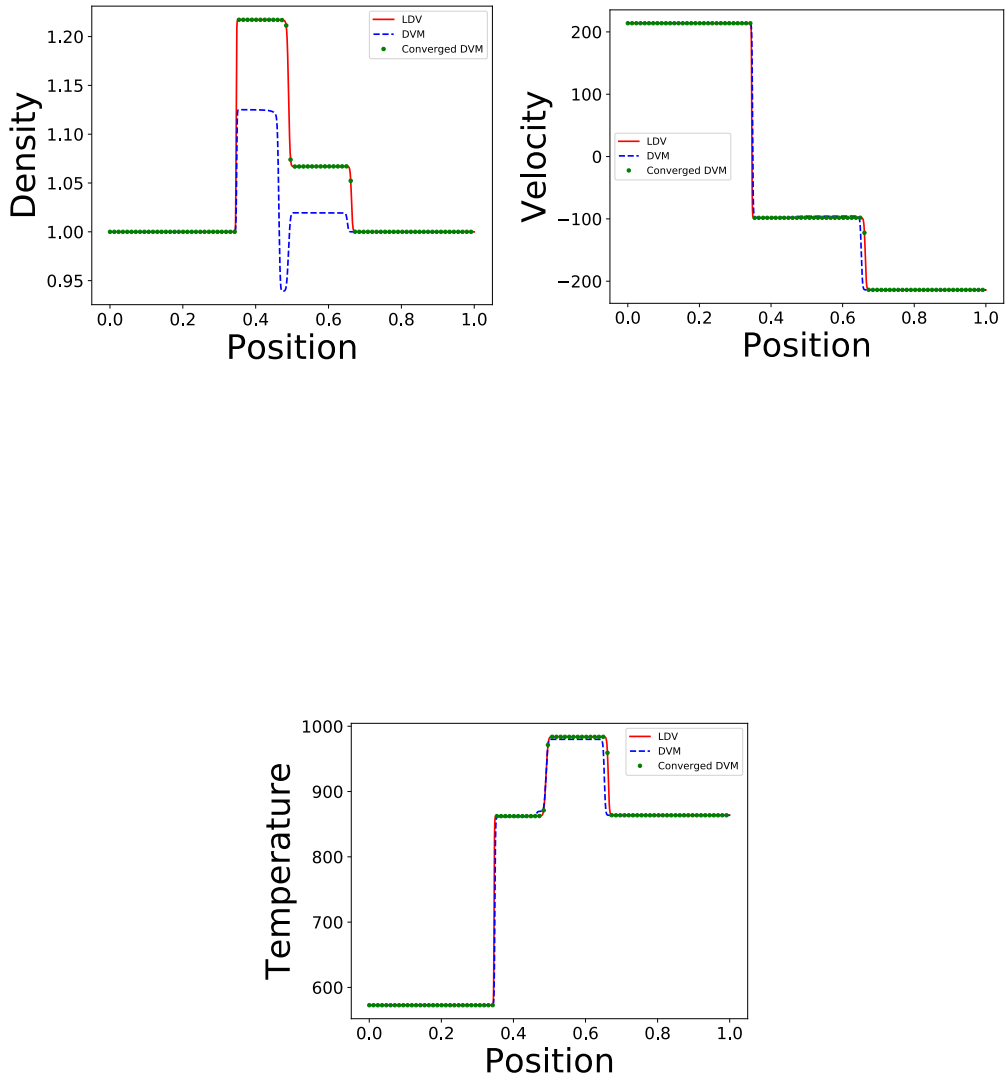

FIGURE 1. Densities, velocities and temperatures of a Riemann problem test case ($K_n = 10^{-3}$) with 2 species with a mass ratio of 10 with 5000 space discretization points, with $l = 5$ and $N_v = 10$ for the LDV case, $l = 4$ and $N_v = 7$ for non-converged DVM and $l = 5$ and $N_v = 30$ for the converged DVM case.

	l	N_v	CPU time
LDV	5	30	279,6s
SLDV	5	30	300,9s
DVM	5	200	516,6s

TABLE 2. Discrete parameters and computation time for test case 5.2 at time $t = 0.008$ s

	l	N_v	CPU time
LDV	5	30	2002s
SLDV	5	30	1710s
DVM	5	200	3456s

TABLE 3. Discrete parameters and computation time for test case 5.2 at time $t = 0.05$

The solution is computed at two different times, firstly at time $t_1 = 0.008$ s, before the shock interaction and secondly at time $t_2 = 0.05$ s, after the shock interaction. The Knudsen number is chosen equal to 10^{-3}. For the pre-interaction solution, results are displayed in figure 2. For the post-interaction solution, see figure 3. Finally, discrete parameters and CPU time are given in tables 2 and 3 .

In this experiment, an important gradient of temperature is initially present. This means that the standard DVM needs to encompass all distributions with only one grid. Hence, an important number of velocities is needed (200). However, the LDV methods works perfectly with only 30 velocities. For the first computation time, the LDV method works better than the SLDV. This can be seen as the consequence of the increase of discrete velocities, which counterbalances the gain in time due to the reduction of the number of interpolations. However, if the computation time is longer, the SLDV method becomes more interesting again. Finally, as for the previous test case, the non-converged DVM method (with the same parameters as the LDV and SLDV methods) is not able to capture correctly the solutions for the first computation time, and even breaks down for the second. The breaking down is explained by the fact that, since a lot of information is not "seen" by the velocity grids, a negative internal energy is obtained. Consequently, this leads to a negative temperature, and thus the impossibility of defining the Maxwellian distribution in such a case.

In ([10]), the discrete velocity grids have been represented after and before the shock. In the present case, the same behaviour of the bounds per species can be observed, depending on the ratio between the temperature and the molecular mass.

5.3. **Shock waves.** For this third case, a two-species gas is considered with particle masses $m^1 = 66,3.10^{-27}$ kg and $m^2 = 20 \times m^1 = 13,26.10^{-25}$ kg. The initial data consists in two shocks interacting with each other at the initial time, with a significant velocity:

$$\begin{cases} \rho^1(t_0,x) = \rho^2(t_0,x) = 1 \text{ kg.m}^{-3}, \\ T^1(t_0,x) = T^2(t_0,x) = 300 \text{ K} , \end{cases}$$

and

$$\begin{cases} u^1(t_0,x) = u^2(t_0,x) = 10^4 \text{ m.s}^{-1} & \text{if } x \in [0,0.5], \\ u^1(t_0,x) = u^2(t_0,x) = -10^4 \text{ m.s}^{-1} & \text{if } x \in [0.5,1]. \end{cases}$$

The solution is computed at time $t = 10^{-5}s$. The Knudsen number is chosen equal to 10^{-5}, which corresponds to fluid regime. Results are displayed in figure 4, and kinetic parameters along with CPU time are given in table 4.

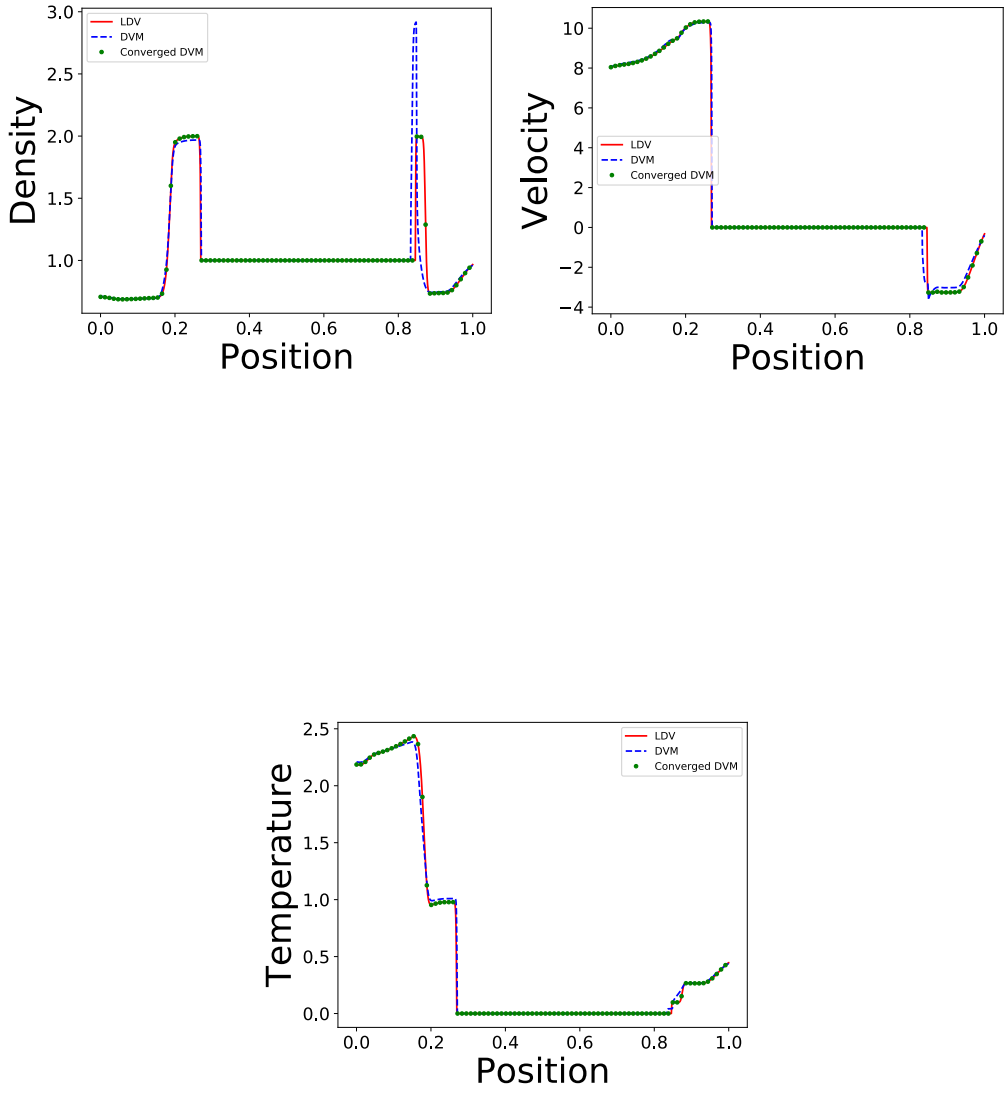

FIGURE 2. Densities, velocities and temperatures of a pre-shock blast waves interaction ($K_n = 10^{-3}$) with 2 species with a mass ratio of 20 with 5000 space discretization points, with $l = 5$ and $N_v = 30$ for the LDV and non-converged DVM cases and $l = 5$ and $N_v = 200$ for the converged DVM case.

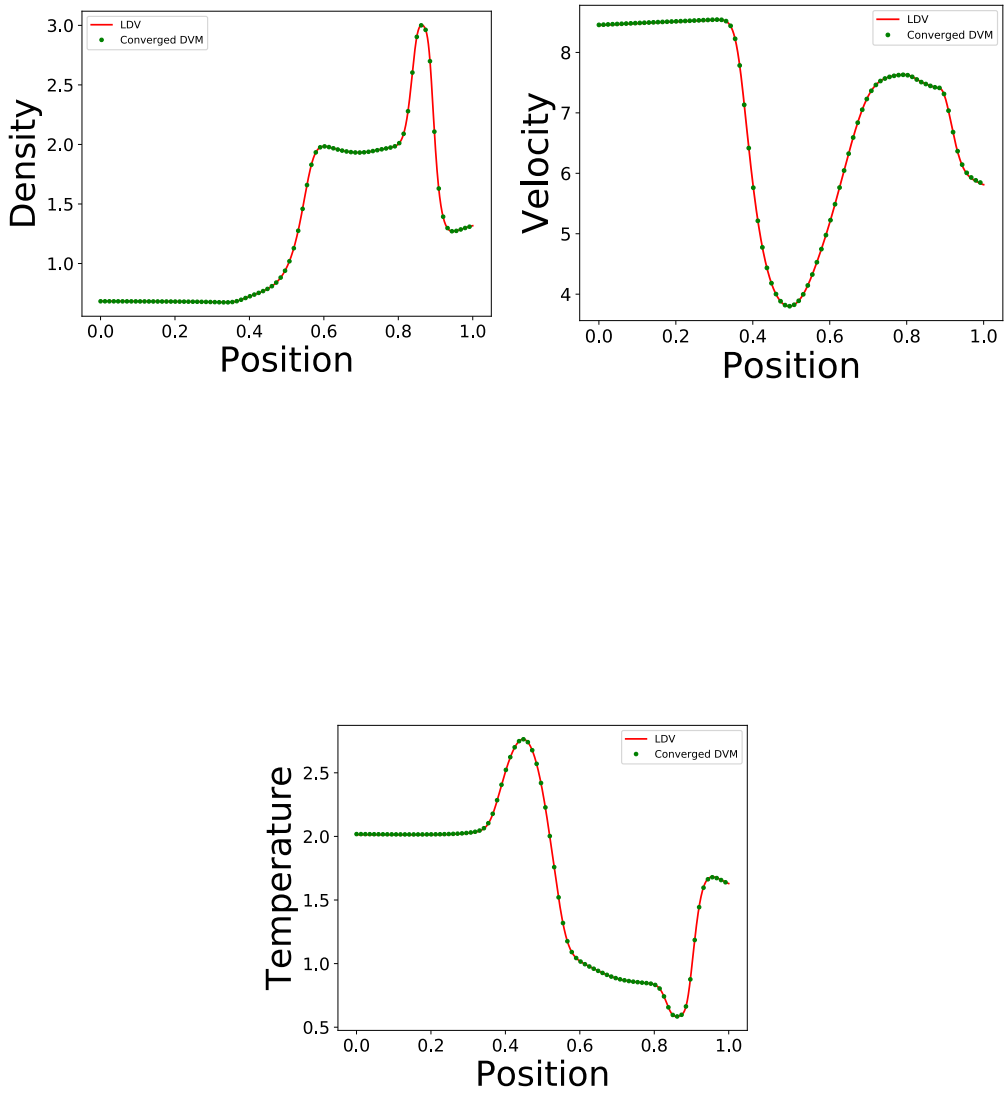

FIGURE 3. Densities, velocities and temperatures of a post-shock blast waves interaction ($K_n = 10^{-3}$) with 2 species with a mass ratio of 20 with 5000 space discretization points, with $l = 5$ and $N_v = 30$ for the LDV case and $l = 5$ and $N_v = 200$ for the converged DVM case.

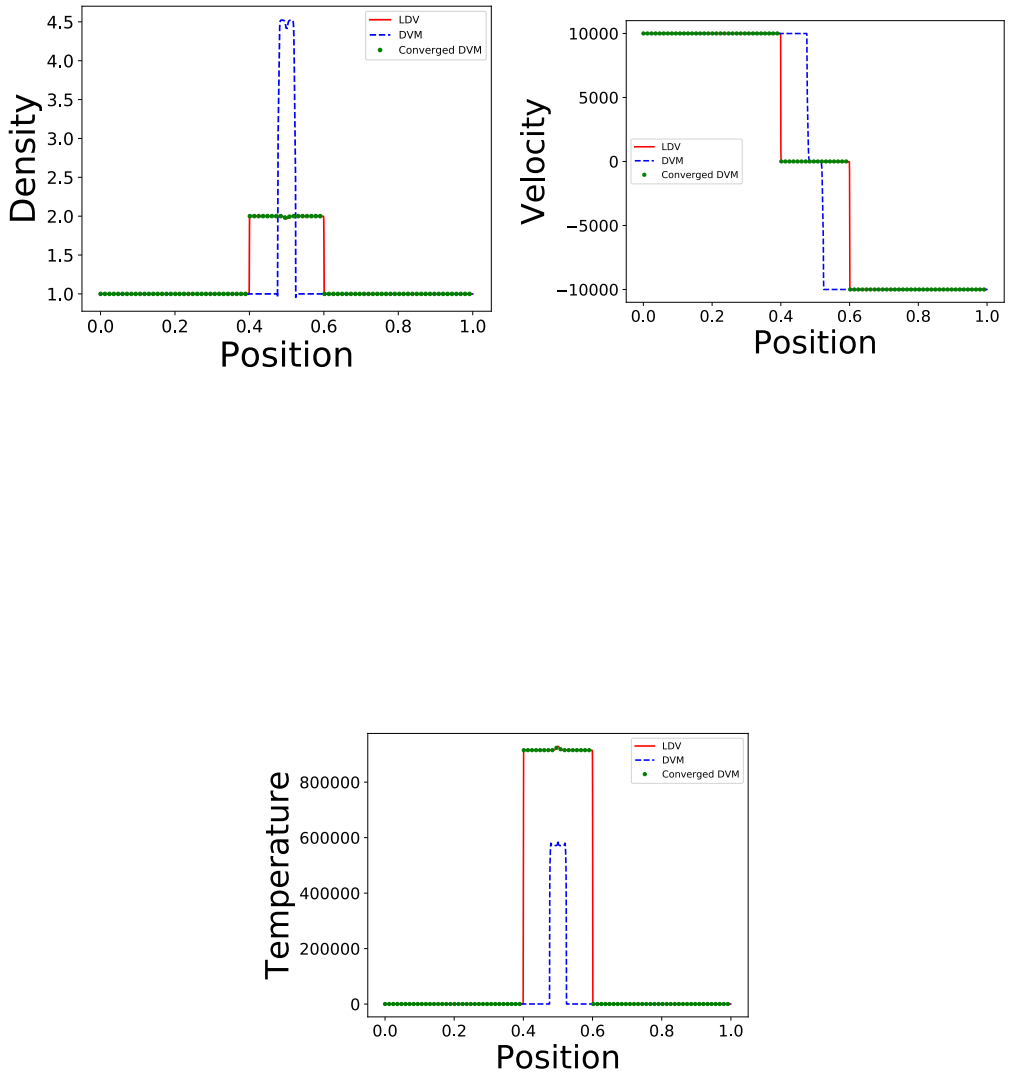

FIGURE 4. Densities, velocities and temperatures of a double shock wave interaction ($K_n = 10^{-5}$) with 2 species with a mass ratio of 20 with 5000 space discretization points, with $l = 5$ and $N_v = 30$ for the LDV and non-converged DVM methods and $l = 180$ and $N_v = 2000$ for the converged DVM case.

	l	N_v	CPU time
LDV	5	30	147s
SLDV	5	30	179s
DVM	180	2000	1824s

TABLE 4. Discrete parameters and computation time for test case 5.3

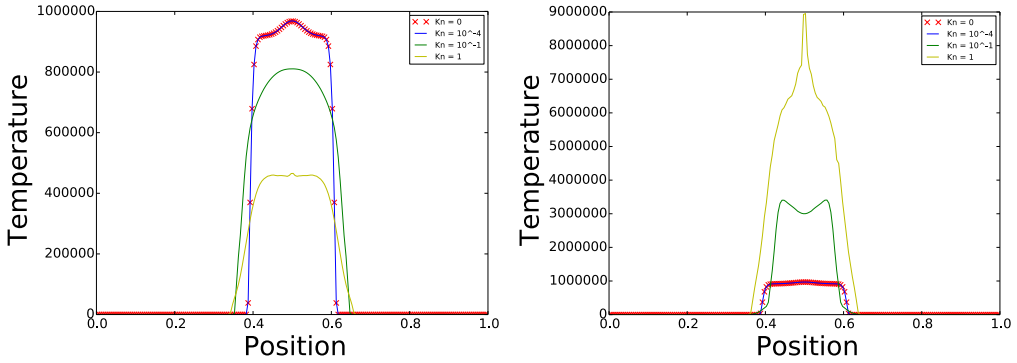

FIGURE 5. Temperatures of a double shock wave interaction for various Knudsen numbers with 2 species with a mass ratio of 20 with 200 space discretization points.

For the LDV and SLDV methods, only 30 discrete velocities are needed, with a domain length of 5. However, for the classical DVM method, a length domain of 180 is necessary in order to compute the solution properly, which requires consequently an important amount of discrete velocities (2000) to mesh this grid. If these requirements are not met, the classical DVM method can be seen to completely fail, as can be seen on all macroscopic quantities.

Concerning CPU times, both adaptive methods are much faster than the DVM method, but the shifted grid method does not seem to allow for a gain of computation time. This can be explained by the same reasons as the previous test case, the increase in the number of discrete velocities during the shifting step increases the computation time.

In figure 5, the temperatures of both species 1 and 2 are displayed, for various values of the Knudsen number. These pictures show the Asymptotic-Preserving behaviour of the method, which allows for the derivation of a method for the Euler system.

5.4. **Sod tube test with high mass ratio.** This objective of this test case is to show the behaviour of the method when applied to particles with mass ratio of the order of those constituting a plasma, namely electrons and ions, with respective particle masses $m^1 = 9,109.10^{-31}$ and $m^2 = 1,627.10^{-27}$, which correspond to a ratio of approximately 2000. The initial data are

	l	N_v	CPU time
LDV	4	30	312s
SLDV	4	30	350s
DVM	20	400	3419s

TABLE 5. Discrete parameters and computation time for test case 5.4

those of a classical Sod tube for densities:

$$\begin{cases} \rho^1(t_0,x) = \rho^2(t_0,x) = 1 \text{ kg.m}^{-3}, & \text{if } x \in [0,0.5], \\ \rho^1(t_0,x) = \rho^2(t_0,x) = 0,125 \text{ kg.m}^{-3}, & \text{if } x \in [0.5,1]. \end{cases}$$

and temperatures:

$$\begin{cases} T^1(t_0,x) = 300, T^2(t_0,x) = 600 \text{ K}, & \text{if } x \in [0,0.5], \\ T^1(t_0,x) = 500, T^2(t_0,x) = 900 \text{ K}, & \text{if } x \in [0.5,1], \end{cases}$$

and the velocity is initially set to zero over the whole domain. The solution is computed at time $t = 2.10^{-6}s$. The Knudsen number is chosen equal to 10^{-7}, which corresponds to fluid regime. Results are displayed in figure 6, and kinetic parameters and CPU time are displayed in table 5.

In this test case, LDV and SLDV methods can be seen to work very well with a length domain of 4 and only 30 discrete velocities. On the other hand, the classical DVM becomes extremely expensive when attempting to obtain converged results. The parameters chosen here ($l = 20$ and $N_v = 400$) allow for the displayed results than can be seen to be still far from being converged (especially densities that are completely wrong), for a computational time that is ten times more important than the time needed to get converged results from adaptive methods.

5.5. **Rarefied heat transfert.** In this test case, a heat transfer problem is considered. It consists in a 2-species gas ($m^1 = 66,3.10^{-27}$ kg, $m^2 = 20.m^1 = 13,26.10^{-25}$ kg) contained in a slab at rest, and the right wall of the slab is heated at a higher temperature that is kept fixed for all time. The initial data are given by:

$$\begin{cases} \rho^1(t_0,x) = \rho^2(t_0,x) = 1 \text{ kg.m}^{-3}, u^1(t_0,x) = u^2(t_0,x) = 0 \text{ m.s}^{-1}, & \forall x \in [0,1], \\ T^1(t_0,x) = T^2(t_0,x) = 300 \text{ K} & \text{if } x \in [0,1[, \\ T^1(t_0,x) = T^2(t_0,x) = 1000 \text{ K} & \text{if } x = 1. \end{cases}$$

On the bounds of the physical domain, a diffusive boundary condition is chosen, which writes, for all α:

$$f^\alpha(x=0,v>0) = \mathcal{M}_{\rho_L,0,T_L}, \qquad f^\alpha(x=1,v>0) = \mathcal{M}_{\rho_R,0,T_R},$$

where $T_L = 300$, $T_R = 1000$ and

$$\rho_L = \frac{\int\limits_{v<0} v f(x=0,v)\mathrm{d}v}{\int\limits_{v>0} v\mathcal{M}_{1,0,T_L}\mathrm{d}v}, \qquad \rho_R = \frac{\int\limits_{v>0} v f(x=1,v)\mathrm{d}v}{\int\limits_{v<0} v\mathcal{M}_{1,0,T_R}\mathrm{d}v},$$

The solution is computed at time $t = 1.3.10^{-3}$ s. The physical domain $[0,1]$ is discretized with $N_x = 1000$ points. The Knudsen is chosen equal to 10, which corresponds to a rarefied regime. To that end, the enlargement procedure presented in section 3.4 is used. Results are displayed in figure 7, and kinetic parameters and CPU time are displayed in table 6.

For this heat transfer test case, the SLDV and LDV methods are seen to both work faster than the DVM method. Moreover, they need a smaller grid and consequently less discrete velocities. Because of the level of rarefaction, oscillations can be witnessed on the results, but they are easily controlled by increasing the number of discrete velocities.

Another advantage of the method is the following: for a given length and number of discrete velocities, the SDLV and LDV methods will give much better results than the DVM method, as

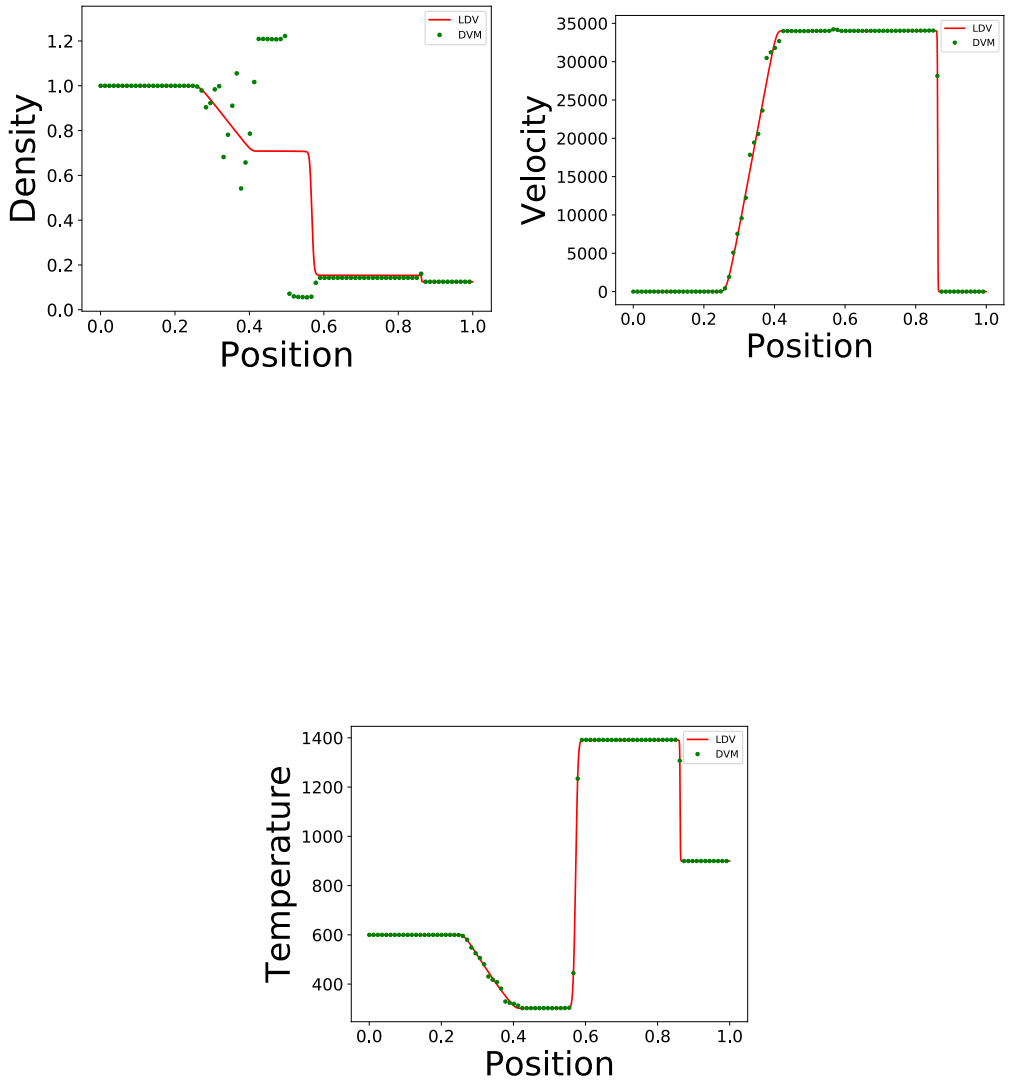

FIGURE 6. Densities, velocities and temperatures of a Sod tube ($K_n = 10^{-7}$) with 2 species with a mass ratio of 2000 with 5000 space discretization points, with $l = 4$ and $N_v = 30$ for the LDV method and $l = 20$ and $N_v = 400$ for the converged DVM case.

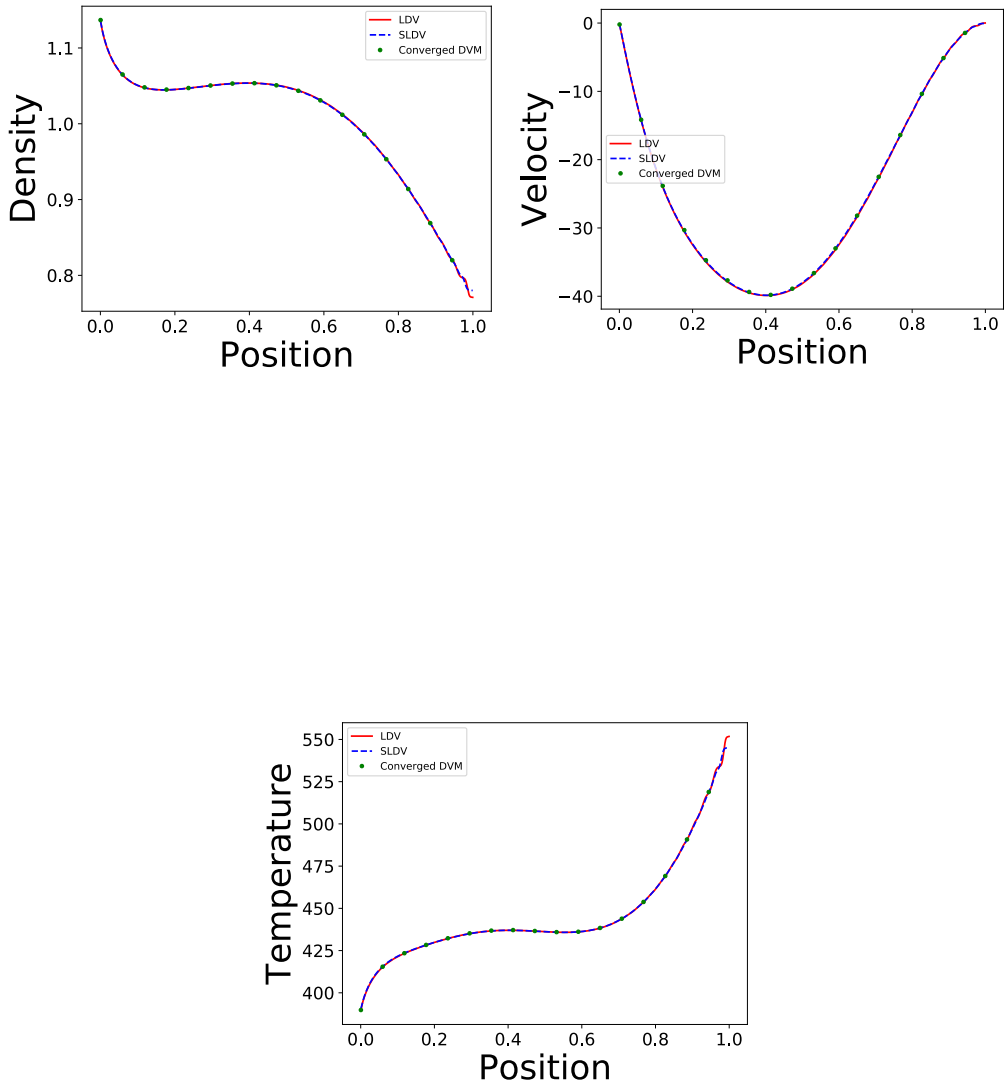

FIGURE 7. Densities, velocities and temperatures of a heat transfer problem ($K_n = 10$) with 2 species with 1000 space discretization points, with $l = 5$ and $N_v = 150$ for the SLDV and LDV cases and $l = 20$ and $N_v = 600$ for the converged DVM case.

	l	N_v	CPU time
LDV	5	150	223s
SLDV	5	150	138s
DVM	20	600	274s

TABLE 6. Discrete parameters and computation time for test case 5.5

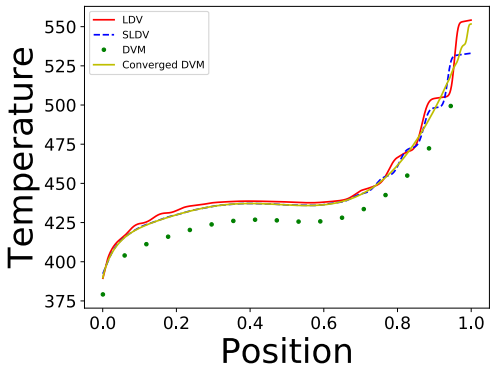

FIGURE 8. Temperatures of a heat transfer problem ($K_n = 10$) with 2 species with 1000 space discretization points, with $l = 4$ and $N_v = 50$ for the LDV, SLDV and DVM cases and $l = 20$ and $N_v = 600$ for the reference DVM case.

can be seen in picture 8. This means that the need for a convergence test is not necessary for our adaptive methods, compared to the DVM method. This highlights the fact that there is a gain in CPU time in the sense that it is not necessary to run the code several times to obtain a satisfying result, while the DVM method needs several executions to find discrete parameters that conveniently fit the problem.

5.6. **Mixture effects.** In this test case, some mixture effects are highlighted for a 2-component gas of respective particle mass $m^1 = 66,3.10^{-27}$ kg, $m^2 = 20.m^1 = 13,26.10^{-25}$ kg. The first component is completely at rest. Its initial data are as follows:

$$\begin{cases} \rho^1(t_0,x) = 1 \text{ kg.m}^{-3}, u^1(t_0,x) = 0 \text{ m.s}^{-1}, & \forall x \in [0,1], \\ T^1(t_0,x) = 300 \text{ K} & \forall x \in [0,1]. \end{cases}$$

The second component is endowed with the following initial data:

$$\begin{cases} \rho^2(t_0,x) = 1 \text{ kg.m}^{-3} & \text{if } x \in [0,0.5[, \\ \rho^2(t_0,x) = 0.125 \text{ kg.m}^{-3} & \text{if } x \in [0.5,1[, \\ T^2(t_0,x) = 300 \text{ K}, u^2(t_0,x) = 0 \text{ m.s}^{-1}, & \forall x \in [0,1], \end{cases}$$

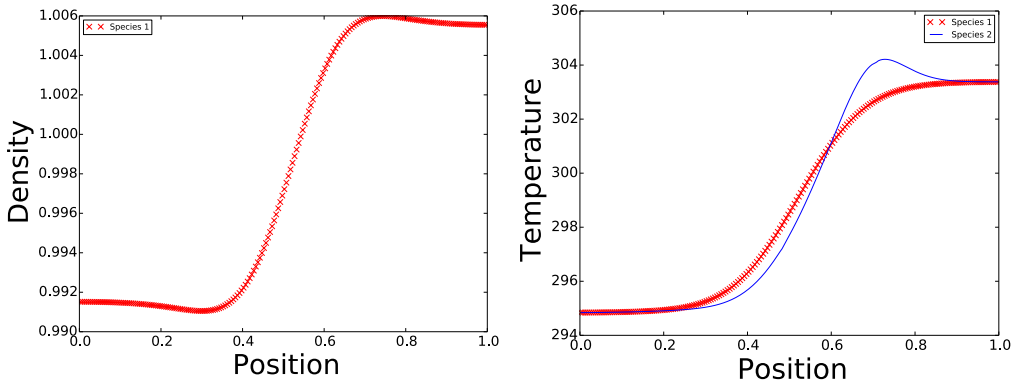

FIGURE 9. Densities and temperatures of a test highlighting mixture effects ($K_n = 10^{-3}$) with 2 species with a mass ratio of 20 with 200 space discretization points.

which correspond to the initial data of a Sod tube test case (with uniform temperature). The domain is discretized with $N_x = 200$ points. The solution is computed at time $t = 10^{-2}$ s. The Knudsen number is chosen equal to 10^{-3}, which corresponds to fluid regime. Results for the density and temperature are displayed in figure 9. To obtain converged results for our method, a grid length of $l = 10$ has been chosen, meshed with $N_v = 100$ points.

As can be seen on the density of species 1 for instance, although initially uniform and at rest, species 1 do not stay in its initial configuration because of the influence of the second component. Similarly, the temperatures can be seen to evolve over time.

6. Conclusion

In this article, an adaptive numerical method is proposed to solve the multi-species kinetic equations for rarefied gases. This method enjoys the property of adapting its discrete velocity grids to the local values of macroscopic velocities and temperatures, and to the particle mass of each species as well. Moreover, it is a dynamic method taking into account the evolution of these quantities over time. A major benefit is that, contrarily to the classical methods using static grids, the computational cost is not increased by the gradients of velocities, temperatures, nor by the disparities of particle masses. However, an important drawback of the method is the computation cost implied by the necessity of performing interpolations to account for the fact that the velocity grids are different for each space point, which can become important as the number of discrete space points increases. A second version of the method is also presented, that is able to circumvent most of the interpolations, by using shifted grids that possess discrete velocities in common, so that interpolations are not required for such points.

A perspective of this work is the application of this method for multi-dimensional flows, where the great number of interpolations enforces the use of such shifted grids. Attempts have been

made in [9] to apply this method to mono-species flows in higher dimension. Moreover, this method is to be applied to other BGK models, such as [11].

7. Acknowledgements

The authors would like to deeply thank Shingo Kosuge and Shigeru Takata for fruitful discussions during the preparation of this paper.

References

[1] P. Andries, K. Aoki, and B. Perthame. A consistent BGK-type model for gas mixtures. *Journal of Statistical Physics*, 106(5-6):993–1018, 2002.
[2] K. Aoki, C. Bardos, and S. Takata. Knudsen Layer for Gas Mixtures. page 27.
[3] R. R. Arslanbekov, V. I. Kolobov, and A. A. Frolova. Kinetic solvers with adaptive mesh in phase space. pages 294–301, Zaragoza, Spain, 2012.
[4] F. Bernard, A. Iollo, and G. Puppo. A Local Velocity Grid Approach for BGK Equation. *Communications in Computational Physics*, 16(4):956–982, Oct. 2014.
[5] P. L. Bhatnagar, E. P. Gross, and M. Krook. A Model for Collision Processes in Gases. I. Small Amplitude Processes in Charged and Neutral One-Component Systems. *Physical Review*, 94(3):511–525, 1954.
[6] G. Bird. *Molecular Gas Dynamics and The Direct Simulation of Gas Flow*. 01 1994.
[7] A. V. Bobylev, M. Bisi, M. Groppi, G. Spiga, and I. F. Potapenko. A general consistent BGK model for gas mixtures. *Kinetic and Related Models*, 11(6), 2018.
[8] S. Brull. An ellipsoidal statistical model for gas mixtures. *Communications in Mathematical Sciences*, 13(1):1–13, 2015.
[9] S. Brull, L. Forestier-Coste, and L. Mieussens. Two dimensional local adaptive discrete velocity grids for rarefied flow simulations. page 180002, Victoria, BC, Canada, 2016.
[10] S. Brull and L. Mieussens. Local discrete velocity grids for deterministic rarefied flow simulations. *Journal of Computational Physics*, 266:22–46, 2014.
[11] S. Brull, V. Pavan, and J. Schneider. Derivation of a BGK model for mixtures. *European Journal of Mechanics - B/Fluids*, 33:74–86, 2012.
[12] C. Cercignani. *The Boltzmann Equation and Its Applications*. Applied Mathematical Sciences. Springer New York, 2012.
[13] S. Chapman, T. Cowling, D. Burnett, and C. Cercignani. *The Mathematical Theory of Non-uniform Gases: An Account of the Kinetic Theory of Viscosity, Thermal Conduction and Diffusion in Gases*. Cambridge Mathematical Library. Cambridge University Press, 1990.
[14] S. Chen, K. Xu, C. Lee, and Q. Cai. A unified gas kinetic scheme with moving mesh and velocity space adaptation. *Journal of Computational Physics*, 231(20):6643–6664, 2012.
[15] S. de Groot and P. Mazur. *Non-equilibrium Thermodynamics*. Dover Books on Physics. Dover Publications, 1984.
[16] F. Filbet and T. Rey. A rescaling velocity method for dissipative kinetic equations. Applications to granular media. *Journal of Computational Physics*, 248:177–199, 2013.
[17] E. P. Gross and M. Krook. Model for Collision Processes in Gases: Small-Amplitude Oscillations of Charged Two-Component Systems. *Physical Review*, 102(3):593–604, 1956.
[18] J. R. Haack, C. D. Hauck, and M. S. Murillo. A Conservative, Entropic Multispecies BGK Model. *Journal of Statistical Physics*, 168(4):826–856, 2017.
[19] B. B. Hamel. Kinetic Model for Binary Gas Mixtures. *Physics of Fluids*, 8(3):418, 1965.
[20] A. Harten and S. Osher. Uniformly high-order accurate nonoscillatory schemes. i. *SIAM Journal on Numerical Analysis*, 24(2):279–309, 1987.
[21] M. T. Ho, L. Wu, I. Graur, Y. Zhang, and J. M. Reese. Comparative study of the Boltzmann and McCormack equations for Couette and Fourier flows of binary gaseous mixtures. *International Journal of Heat and Mass Transfer*, 96:29–41, 2016.
[22] S. Jaiswal, A. A. Alexeenko, and J. Hu. A discontinuous Galerkin fast spectral method for the multi-species Boltzmann equation. *Computer Methods in Applied Mechanics and Engineering*, 352:56–84, 2019.
[23] S. Jaiswal, A. Pikus, A. Strongrich, I. B. Sebastiao, J. Hu, and A. Alexeenko. Quantification of thermally-driven flows in microsystems using Boltzmann equation in deterministic and stochastic contexts.
[24] C. Klingenberg, M. Pirner, and G. Puppo. A consistent kinetic model for a two-component mixture of polyatomic molecules. *arXiv:1806.11486 [math]*, 2018.
[25] V. Kolobov and R. Arslanbekov. Towards adaptive kinetic-fluid simulations of weakly ionized plasmas. *Journal of Computational Physics*, 231(3):839–869, 2012.
[26] S. Kosuge. Model Boltzmann equation for gas mixtures: Construction and numerical comparison. *European Journal of Mechanics - B/Fluids*, 28(1):170–184, 2009.

[27] S. Kosuge, H. Mizuno, and K. Aoki. Numerical Investigation on Models of the Boltzmann Equation for Gas Mixtures. *Rarefied Gas Dynamics*, page 6, 2007.
[28] C. Liu and K. Xu. A unified gas kinetic scheme for continuum and rarefied flows v: Multiscale and multi-component plasma transport. *Communications in Computational Physics*, 22(5):1175–1223, 2017.
[29] F. J. McCormack. Construction of linearized kinetic models for gaseous mixtures and molecular gases. *Physics of Fluids*, 16(12):2095, 1973.
[30] T. F. Morse. Kinetic Model Equations for a Gas Mixture. *Physics of Fluids*, 7(12):2012, 1964.
[31] C.-W. Shu. Essentially non-oscillatory and weighted essentially non-oscillatory schemes for hyperbolic conservation laws. In A. Quarteroni, editor, *Advanced Numerical Approximation of Nonlinear Hyperbolic Equations*, volume 1697, pages 325–432. Springer Berlin Heidelberg, Berlin, Heidelberg, 1998.
[32] L. Sirovich. Kinetic Modeling of Gas Mixtures. *Physics of Fluids*, 5(8):908, 1962.
[33] R. Wang and K. Xu. Unified gas-kinetic scheme for multi-species non-equilibrium flow. In *AIP Conference Proceedings*, volume 1628, pages 970–975. AIP, 2014.
[34] T. Xiao, K. Xu, and Q. Cai. A unified gas-kinetic scheme for multiscale and multicomponent flow transport. *Applied Mathematics and Mechanics*, 40(3):355–372, 2019.
[35] S. Zabelok, R. Arslanbekov, and V. Kolobov. Adaptive kinetic-fluid solvers for heterogeneous computing architectures. *Journal of Computational Physics*, 303:455–469, 2015.
[36] Y. Zhang, L. Zhu, P. Wang, and Z. Guo. Discrete unified gas kinetic scheme for flows of binary gas mixture based on the McCormack model. *Physics of Fluids*, 31(1):017101, 2019.
[37] Y. Zhang, L. Zhu, R. Wang, and Z. Guo. Discrete unified gas kinetic scheme for all Knudsen number flows. III. Binary gas mixtures of Maxwell molecules. *Physical Review E*, 97(5), 2018.

IMB
E-mail address: stephane.brull@math.u-bordeaux.fr

IMB
E-mail address: corentin.prigent@math.u-bordeaux.fr